# Docking of Syk to FcεRI is enhanced by Lyn but limited in duration by SHIP1

William K. Kanagy[a], Cédric Cleyrat[a,b], Mohamadreza Fazel[c], Shayna R. Lucero[a], Marcel P. Bruchez[d], Keith A. Lidke[b,c], Bridget S. Wilson[a,b], and Diane S. Lidke[a,b,*]

[a]Department of Pathology, [b]Comprehensive Cancer Center, and [c]Department of Physics, University of New Mexico, Albuquerque, NM 87131; [d]Department of Biological Sciences and Department of Chemistry, Carnegie Mellon University, Pittsburgh, PA 15213

**ABSTRACT** **The high-affinity immunoglobulin E (IgE) receptor, FcεRI, is the primary immune receptor found on mast cells and basophils. Signal initiation is classically attributed to phosphorylation of FcεRI β– and γ-subunits by the Src family kinase (SFK) Lyn, followed by the recruitment and activation of the tyrosine kinase Syk. FcεRI signaling is tuned by the balance between Syk-driven positive signaling and the engagement of inhibitory molecules, including SHIP1. Here, we investigate the mechanistic contributions of Lyn, Syk, and SHIP1 to the formation of the FcεRI signalosome. Using Lyn-deficient RBL-2H3 mast cells, we found that another SFK can weakly monophosphorylate the γ-subunit, yet Syk still binds the incompletely phosphorylated immunoreceptor tyrosine-based activation motifs (ITAMs). Once recruited, Syk further enhances γ-phosphorylation to propagate signaling. In contrast, the loss of SHIP1 recruitment indicates that Lyn is required for phosphorylation of the β-subunit. We demonstrate two noncanonical Syk binding modes, *trans* γ-bridging and direct β-binding, that can support signaling when SHIP1 is absent. Using single particle tracking, we reveal a novel role of SHIP1 in regulating Syk activity, where the presence of SHIP1 in the signaling complex acts to increase the Syk:receptor off-rate. These data suggest that the composition and dynamics of the signalosome modulate immunoreceptor signaling activities.**

**Monitoring Editor**
Avery August
Cornell University

Received: Dec 9, 2021
Revised: Jun 23, 2022
Accepted: Jun 28, 2022

## INTRODUCTION

The ultimate outcome of membrane-associated signaling is tuned by a combination of both positive and negative downstream signaling molecules that direct the cellular response. Immunoreceptors share a general mechanism of activation whereby receptor–antigen engagement initiates the formation of a signaling complex, or signalosome, to promote the recruitment and interaction of positive and negative signaling molecules (Turner and Kinet, 1999; Siraganian *et al.*, 2002, 2010; Sigalov, 2004; Kalesnikoff and Galli, 2008; Geahlen, 2009; Chakraborty and Weiss, 2014; Suzuki, 2017). The Fc receptors, T-cell receptor (TCR) and B-cell receptor (BCR), are members of the family of multichain immune-recognition receptors (MIRR) that share this common process. MIRRs lack intrinsic kinase activity, relying instead on the recruitment of signaling molecules to phosphorylated tyrosines in the associated immunoreceptor tyrosine-based activation motifs (ITAMs). Initial phosphorylation of receptor ITAMs is attributed to Src family kinases (SFKs), such as Lyn (Fc receptors, BCR) and Lck (TCR). The ITAM phosphotyrosines (pTyr) provide binding sites for the recruitment of both activating and inhibitory molecules through their SH2 domains. Engagement of Syk/Zap-70 via their two SH2 domains is critical for propagation of positive signaling from MIRRs (Hatada *et al.*, 1995; Zhang *et al.*, 1996; Siraganian *et al.*, 2002, 2010; Deindl *et al.*, 2007). While TCR signaling depends on Zap-70, Syk is more ubiquitously expressed and plays roles in multiple signaling cascades, including Fc receptors, hemITAMs, CD74, and integrins (Suzuki *et al.*, 2000; Starlets *et al.*, 2006; Hughes *et al.*, 2010; Bauer and Steinle, 2017; Antenucci *et al.*, 2018). The flexibility of Syk functionality is further demonstrated by

This article was published online ahead of print in MBoC in Press (http://www.molbiolcell.org/cgi/doi/10.1091/mbc.E21-12-0603) on July 6, 2022.

*Address correspondence to: Diane Lidke (dlidke@salud.unm.edu).

Abbreviations used: BAMF, Bayesian multiple-emitter fitting; BCR, B-cell receptor; BSA, bovine serum albumin; DNP, dinitrophenyl; GFP, green fluorescent protein; IgE, immunoglobulin E; ITAM, immunoreceptor tyrosine–based activation motif; KO, knockout; MIRR, multichain immunorecognition receptors; mNG, mNeonGreen; pTyr, phosphorylated tryosine; SFK, Src family kinase; SH2, Src homology 2; SHIP1, SH2 domain-containing inositol phosphatase 1; SPT, single-particle tracking; SYFP2, super yellow fluorescent protein 2; Syk, spleen tyrosine kinase; TCR, T-cell receptor; TIRF, total internal reflection fluorescence; WT, wild type.

its ability to substitute for Zap-70 in T-cells and propagate TCR signaling without the need for Lck (Chu *et al.*, 1996). The positive ITAM-based signaling is regulated by negative signaling molecules, including protein (SHP1 and SHP2) and lipid (SHIP1) phosphatases that are also recruited to phospho-ITAMs (Ono *et al.*, 1996; Li *et al.*, 1999; Furumoto *et al.*, 2004; Chong and Maiese, 2007). Therefore, the dynamics and composition of the signalosome are critical determinants in directing the cell signaling response.

Despite this common model, questions remain regarding the exact molecular mechanisms that regulate ITAM signaling. For example, receptor clustering has been considered an important step in MIRR activation, but the impact of receptor number and spacing within clusters is not understood and for the TCR it has been suggested that even a single peptide:TCR complex can trigger signal propagation (Yokosuka *et al.*, 2005; Kim *et al.*, 2006; Krogsgaard *et al.*, 2007; Andrews *et al.*, 2009; Huang *et al.*, 2013; Mukherjee *et al.*, 2013; Shelby *et al.*, 2013; Chakraborty and Weiss, 2014). ITAM conformational changes (Shi *et al.*, 2012; Ma *et al.*, 2017) and mechanotransduction (Brazin *et al.*, 2018; Feng *et al.*, 2018) may also have regulatory roles. Furthermore, the number of associated subunits, ITAM repeats per subunit, and variations in ITAM sequence can all potentially influence interactions with downstream proteins. The related family of hemITAM receptors function in a manner similar to that of MIRRs, with the exception that the hemITAM sequence contains a single tyrosine and cannot support Syk binding in *cis*. The absolute requirement for SFKs in ITAM phosphorylation is also not clear, because multiple studies have shown that Syk is also capable of phosphorylating ITAM/hemITAM tyrosines, independent of SFKs (Takata *et al.*, 1994; Rolli *et al.*, 2002; Rogers *et al.*, 2005; Huysamen *et al.*, 2008; Mukherjee *et al.*, 2013; Bauer *et al.*, 2017). Thus, ITAM signaling is more complex than the classically described model.

To better understand ITAM-based signaling, we have characterized the interplay between ITAM phosphorylation requirements and the dynamics and composition of the FcεRI signalosome. Aggregation of FcεRI by multivalent antigen initiates a signaling cascade that ultimately leads to mast cell degranulation and cytokine production, which is often associated with allergy and asthma. FcεRI consists of three ITAM-containing subunits, a disulfide-linked γ-dimer, and the β-subunit, coupled to the immunoglobulin E (IgE)-binding α-subunit. Lyn is considered to be the dominant SFK in mast cells that phosphorylates both the γ and β ITAMs upon receptor aggregation, facilitating the binding of the SH2 domains of downstream proteins to the pTyr (Wilson *et al.*, 1995; Gaul *et al.*, 2000; Furumoto *et al.*, 2004; Xiao *et al.*, 2005). The γ ITAMs are primarily associated with the recruitment of Syk, where the two SH2 domains of Syk are proposed to bind a doubly phosphorylated γ-subunit in *cis* (Narula *et al.*, 1995; Fütterer *et al.*, 1998; Yamashita *et al.*, 2008). Recently, we used structural γ-mutants and computational modeling to demonstrate that γ ITAMs are capable of stimulating a calcium response even when the phosphorylation profile is incomplete, such that the two Syk SH2 domains must bridge the C-terminal pTyr of the γ-dimer in *trans* (Travers *et al.*, 2019). This previously undescribed *trans* binding confirmed the requirement of two pTyr to enable Syk docking. We have also shown that the dynamics of receptor:Syk interactions are tightly regulated. Using a Syk mutant with altered receptor binding kinetics, we demonstrated that a small change in the binding off-rate of Syk to FcεRI can dramatically alter mast cell signaling outcomes (Schwartz *et al.*, 2017). The β-subunit, on the other hand, is associated with negative regulation of signaling through the recruitment of phosphatases, such as SHIP1 (Kimura *et al.*, 1997; Furumoto *et al.*, 2004). Studies have shown that at both sub- and supraoptimal antigen doses, SHIP1 phosphorylation is increased and is more strongly associated with FcεRI aggregates, compared with optimal antigen concentrations (Mahajan *et al.*, 2014). Phosphorylation of the β ITAM is also enhanced with increasing antigen concentrations and is coupled to a stronger association with both Lyn and SHIP1 (Gimborn *et al.*, 2005; Xiao *et al.*, 2005).

In this study, we evaluate the contributions of Lyn, Syk, and SHIP1 in shaping FcεRI signaling. We show that in the absence of Lyn, the γ ITAM is incompletely phosphorylated, but still able to recruit Syk. Once recruited, Syk further phosphorylates FcεRIγ to a level that supports degranulation. Syk does not phosphorylate the β ITAM, resulting in a loss of SHIP1 recruitment in cells lacking Lyn, such that negative regulation is sufficiently reduced to allow for weak signaling to propagate. We reveal an unexpected role for SHIP1 in regulating Syk activity, where the presence of SHIP1 in the FcεRI signaling complex acts to reduce Syk:ITAM binding lifetime and limits the extent of Syk phosphorylation. This work provides new insights into the coordination of proteins within the signalosome that balance positive and negative signaling.

## RESULTS

### Antigen-induced FcεRI signaling is altered but not lost in RBL-Lyn$^{KO}$ cells

We began by generating a Lyn knockout cell line in RBL-2H3 cells (RBL-Lyn$^{KO}$) using CRISPR-Cas9 gene editing. Several subclones deficient in Lyn were successfully generated (Figure 1A; see *Materials and Methods* for details on characterization of knockout cells). Previous work in bone marrow mast cells had shown that Fyn can substitute for Lyn and facilitate FcεRI signaling (Parravicini *et al.*, 2002; Hernandez-Hansen *et al.*, 2004); however, RBL cells lack Fyn expression (Sanderson *et al.*, 2010). It was, therefore, unexpected to find that each of the RBL-Lyn$^{KO}$ cell lines maintained a robust degranulation response upon FcεRI cross-linking with multivalent antigen (Figure 1B). Figure 1B shows the degranulation response of RBL-Lyn$^{KO}$ subclone cells over a range of antigen ($DNP_{25}$-BSA, valency of 25) doses in comparison to wild type (WT) RBL cells. Clone BB3 was selected for further studies. Knockout of Lyn did not alter surface levels of FcεRI as measured by flow cytometry (Figure 1C).

Consistent with the ability to release granular contents, we also observed a calcium response upon FcεRI cross-linking. Calcium mobilization was measured by loading cells with the ratiometric calcium indicator dye Fura-2, as described previously (Schwartz *et al.*, 2017; Travers *et al.*, 2019). Heat maps shown in Figure 1D report the responses for $n \geq 65$ cells per condition. Addition of $DNP_{25}$-BSA leads to an increase in cytosolic calcium for both cell types. However, the RBL-Lyn$^{KO}$ calcium response was lower in magnitude and delayed when compared with that of RBL-WT cells (Figure 1, E and F). These results demonstrate that mast cell signaling can occur in the absence of Lyn and Fyn, raising new questions about the molecular mechanisms that support FcεRI signaling in RBL-Lyn$^{KO}$ cells.

### Syk enhances FcεRIγ phosphorylation to propagate signaling in RBL-Lyn$^{KO}$ cells

To investigate the early signaling events in RBL-Lyn$^{KO}$ cells, we examined the phosphorylation state of the FcεRI γ-subunit using Western blot analysis. FcεRI was immunoprecipitated using an anti-IgE antibody, which coprecipitates the α-, β-, and γ-subunits. Previous work by the Rivera lab (Yamashita *et al.*, 2008) has shown that, by preparing lysates in nonreducing sample buffer, the FcεRIγ dimer is preserved, with the γ-dimers separating on the gel as a function of pTyr patterns (0–4 possible pTyr per dimer). The immunoblots in Figure 2 show that the full phosphorylation profile presents as four separate bands that migrate above the nonphosphorylated γ-dimer

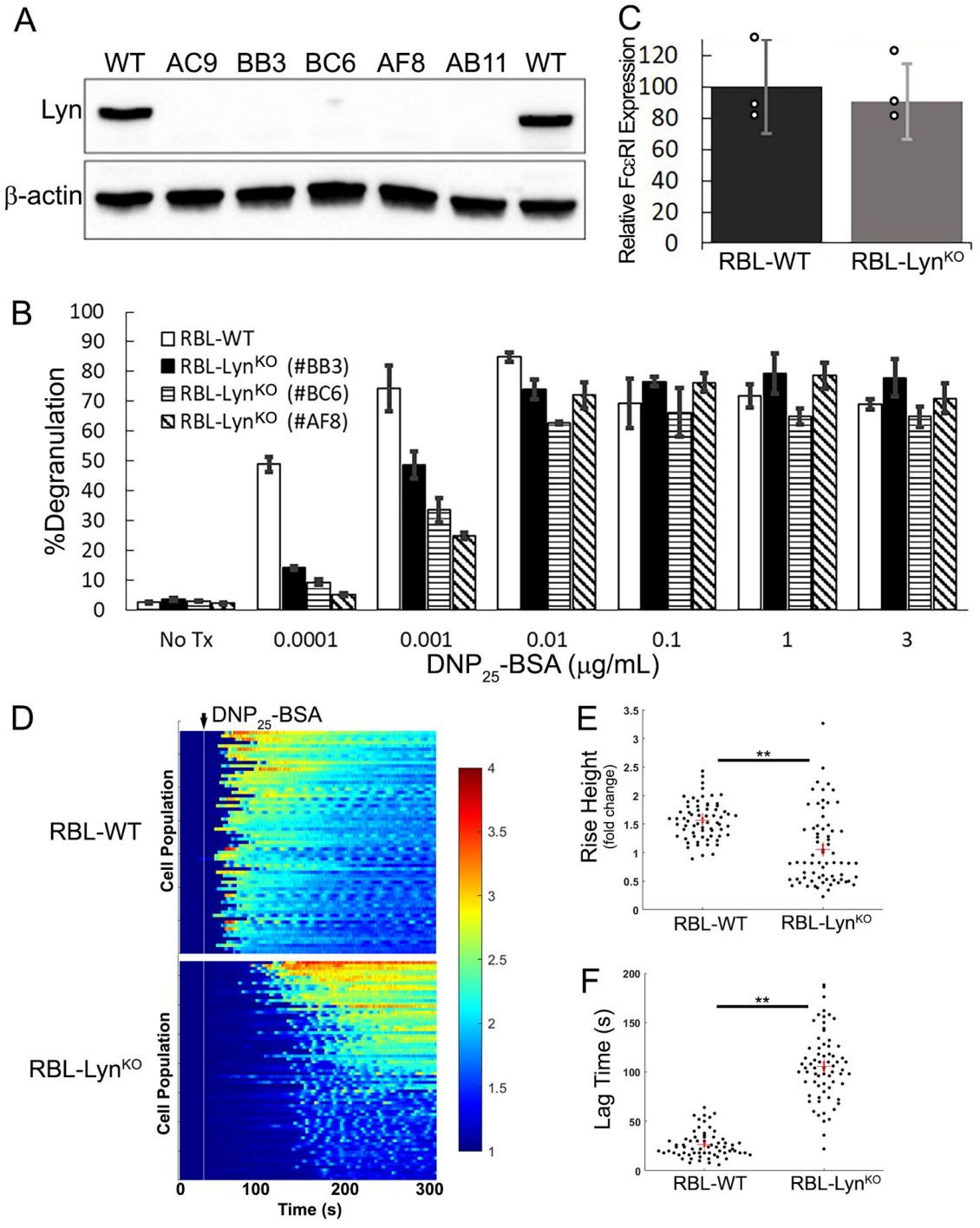


FIGURE 1: FcεRI signaling occurs in the absence of Lyn. (A) Immunoblot of whole cell lysates from RBL-WT or RBL-Lyn$^{KO}$ subclones showing successful CRISPR-Cas9 knockout of Lyn. Unless specified, subclone "BB3" was used for subsequent studies. Representative blot from two independent sample preparations. (B) Degranulation was measured by relative β-hexosaminidase released after 30 min of incubation with $DNP_{25}$-BSA at the respective concentrations. Average values from three different experiments, with each treatment run in duplicate for each experiment; mean ± SD. (C) Knockout of Lyn does not alter FcεRI membrane surface levels. Cells were labeled with IgE-AF647 overnight and analyzed by flow cytometry. SEM of mean fluorescence intensity (MFI) values normalized to WT levels; three independent trials. (D) Calcium release in RBL-WT or -Lyn$^{KO}$ cells after activation with 0.1 μg/ml $DNP_{25}$-BSA. Heatmaps indicate increased calcium release as the Fura-2 ratio increases from baseline (blue to red), with each line representing the calcium ratio over time for a single cell. RBL-WT $n = 67$, RBL-Lyn$^{KO}$ $n = 65$. (E, F) Quantification of calcium response curves in D to extract the relative increase in the Fura-2 ratio per cell after antigen cross-linking (rise height; E) and the time between antigen addition and calcium release (lag time; F). Red cross and error bars report the mean and SEM, respectively. ** $P < 0.0001$ from two-sample Kolmogorov–Smirnov test.

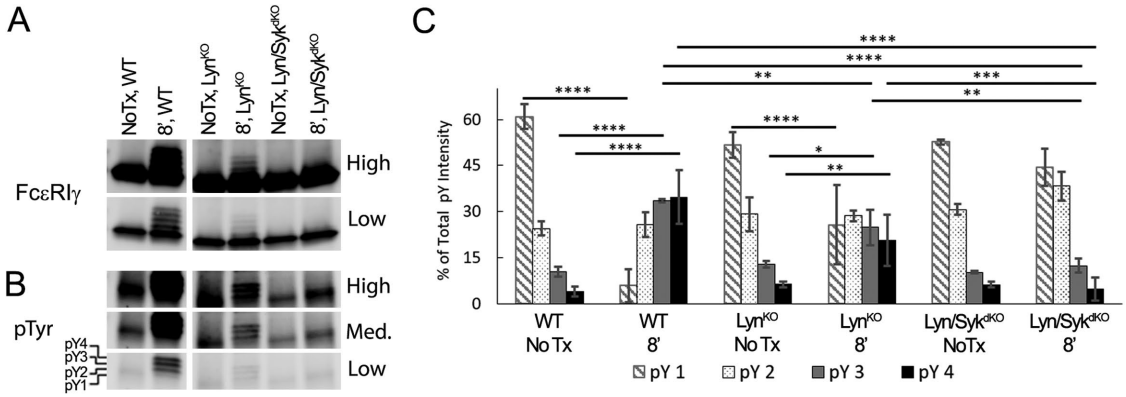


**FIGURE 2:** Syk activity is required for enhanced phosphorylation of FcεRIγ ITAMs in RBL-Lyn$^{KO}$ cells.
(A, B) Representative immunoblots probed for (A) total FcεRIγ or (B) phosphorylation (pTyr) comparing RBL-WT, -Lyn$^{KO}$, and -Lyn/Syk$^{dKO}$ cells before (No Tx) or after 8 min of 1 μg/ml $DNP_{25}$-BSA cross-linking. Blots are displayed with different contrasts (low, medium, high) to visualize lower levels of ITAM phosphorylation in the knockout cells. pY1, pY2, pY3, and pY4 indicate the band corresponding to the respective number of phosphotyrosines in the γ-dimer.
(C) Quantification of the immunoblots described in B to determine the percentage that each pTyr FcεRIγ band contributes to total FcεRIγ phosphorylation. (mean ± SD); No Tx $n = 3$, +8′ $DNP_{25}$-BSA $n = 5$. **** $P < 0.0001$, *** $P < 0.001$, ** $P < 0.01$, * $P < 0.05$, analysis of variance (ANOVA) with Tukey's multiple comparisons test.

in response to antigen stimulation. This banding can be observed using either anti-γ (Figure 2A) or anti-pTyr (Figure 2B) antibodies. Using this approach, we compared γ-phosphorylation for RBL-WT and RBL-Lyn$^{KO}$ cells. Considering the reports that Syk is capable of phosphorylating BCR ITAMs (Rolli *et al.*, 2002), we also examined RBL cells with both Lyn and Syk knocked out (RBL-Lyn\Syk$^{dKO}$). The RBL-Lyn\Syk$^{dKO}$ cell line was produced using CRISPR-Cas9 to knock out Syk in the RBL-Lyn$^{KO}$ cells. We observed that the extent of γ-phosphorylation is significantly reduced in RBL-Lyn$^{KO}$ cells; however, the banding pattern was still present (Figure 2, A and B). In Figure 2C, we quantified the γ-phosphorylation patterns for each cell type by plotting the intensity of phosphorylation for each band (pY1, pY2, pY3, pY4 seen in Figure 2B) normalized to the total phosphorylation within each condition. In resting cells, the γ-dimer is primarily found in low phosphostates (pY1, pY2). After antigen cross-linking, RBL-WT cells show a shift to higher γ-phosphostates (pY3, pY4). Stimulated RBL-Lyn$^{KO}$ cells also show a shift to higher γ-phosphorylation bands. Remarkably, in RBL-Lyn\Syk$^{dKO}$ cells there is a very slight increase in pY2, though not significant, while the higher phosphorylation states of the γ-dimer are completely lost. This indicates that Syk is the primary kinase acting to increase γ ITAM phosphorylation in RBL-Lyn$^{KO}$ cells, consistent with in vitro studies showing that the FcεRIγ ITAM is a substrate for Syk (Kihara and Siraganian, 1994; Shiue *et al.*, 1995).

### SFK phosphorylation of FcεRI is needed for Syk recruitment

The above results show that Syk can phosphorylate the γ ITAM. However, it was unclear whether Syk might act on the γ-tyrosines from the cytosol, a possibility suggested by other reports (Rolli *et al.*, 2002; Mukherjee *et al.*, 2013), or instead the incomplete γ-phosphorylation seen in the absence of Syk and Lyn (Figure 2) was sufficient to enable initial Syk docking. To differentiate between these possibilities, we introduced a fluorescently (SYFP2)-tagged Syk truncation mutant that retains both SH2 domains but lacks the kinase domain (Syk(SH2)-SYFP2) into RBL-Lyn/Syk$^{dKO}$ cells. Upon receptor aggregation, Syk(SH2)-SYFP2 accumulated at the plasma membrane in clusters that colocalized with aggregated IgE-AF647-FcεRI (Figure 3A and Supplemental Figure S1). Syk(SH2)-SYFP2 recruitment to receptor aggregates was prevented by treatment with 0.1 μM dasatinib, an inhibitor of SFK kinase activity (Figure 3B and Supplemental Figure S1). Consistent with a loss of Syk recruitment, we also found that in RBL-Lyn$^{KO}$ cells γ-phosphorylation and degranulation were reduced by dasatinib in a dose-dependent manner and completely abrogated at 0.1 μM dasatinib (Supplemental Figure S2). These results indicate that a dasatinib-sensitive kinase other than Lyn/Fyn can initiate weak γ–phosphorylation, priming the ITAM for Syk-SH2 binding. Work by others has shown that Lck can phosphorylate FcεRI when expressed in Jurkat T-cells (Adamczewski *et al.*, 1995). Immunoblotting confirmed that, while Fyn was indeed absent in RBL cells (Sanderson *et al.*, 2010), Src and Lck were detectable (Supplemental Figure S3A), as previously reported. We found that overexpression of Lck or Src in RBL-Lyn$^{KO}$ cells recovered FcεRIγ and Syk phosphorylation in response to antigen cross-linking (Supplemental Figure S3, B and C). These results support a model for signaling in RBL-Lyn$^{KO}$ cells where Syk can amplify phosphorylation of the γ ITAM in a feedforward mechanism, but only after another SFK elicits low-level ITAM phosphorylation (barely detectable by Western blot) to enable Syk recruitment via SH2 binding (Johnson *et al.*, 1995; Kimura *et al.*, 1996b; Faeder *et al.*, 2003; Yamashita *et al.*, 2008).

### Syk recruitment is enhanced by Lyn

The changes in calcium response and the reduced γ ITAM phosphorylation observed in RBL-Lyn$^{KO}$ cells indicated that, despite passing the threshold needed to support degranulation, FcεRI signaling in RBL-Lyn$^{KO}$ cells is impaired. Because Syk is a critical node in the signaling pathway, we used confocal microscopy to record Syk recruitment to FcεRI aggregates. As described previously, we expressed Syk-tagged with mNeonGreen (Syk-mNG) in RBL cells deficient of endogenous Syk (RBL-Syk$^{KO}$ or RBL-Lyn/Syk$^{dKO}$) and monitored Syk-mNG recruitment to FcεRI aggregates (Schwartz *et al.*, 2017). As expected, Syk-mNG colocalizes with FcεRI aggregates within 1 min of cross-linking (Figure 4A and Supplemental Figure S1). In RBL-Lyn$^{KO}$ cells, Syk recruitment to receptor aggregates was markedly delayed, becoming visible only after 3 min (Figure 4B and Supplemental Figure S1; see also Figure 5C). To further quantify Syk recruitment and receptor aggregation, Total internal reflection fluorescence (TIRF) microscopy was used to acquire

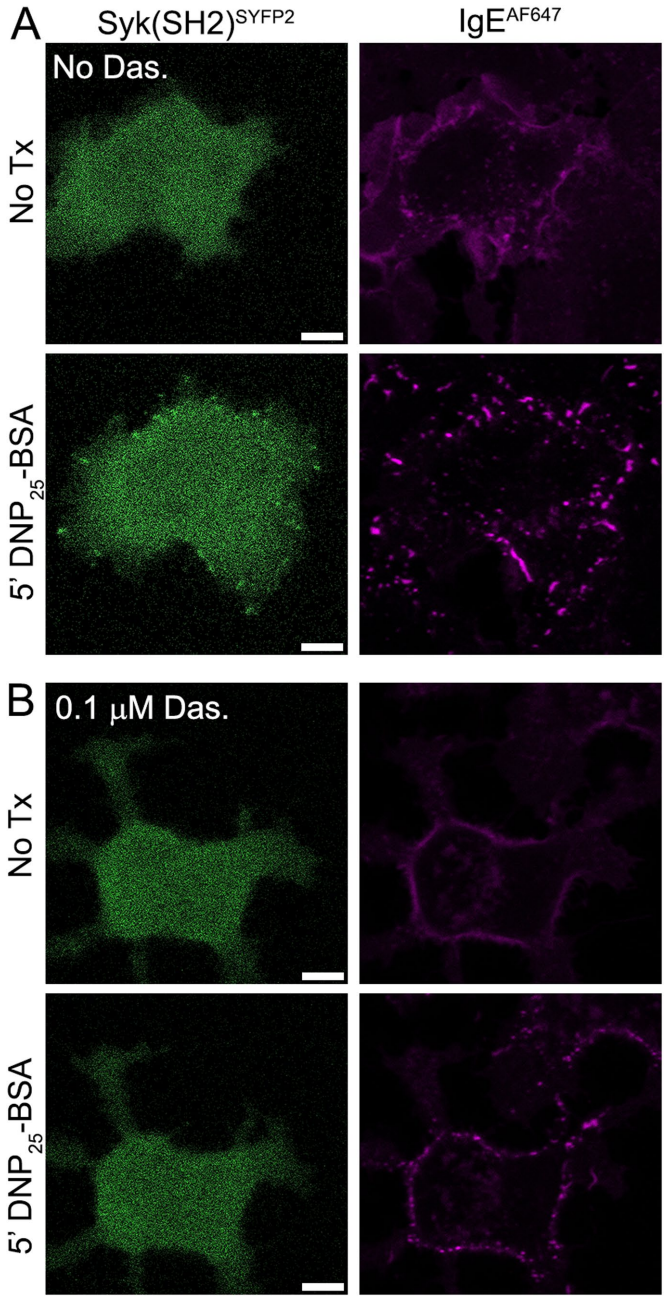


FIGURE 3: ITAM phosphorylation by an SFK is required before Syk recruitment. (A) Syk(SH2)$^{SYFP2}$, which retains both SH2 domains but lacks the kinase domain, is recruited to FcεRI aggregates in RBL-Lyn/Syk$^{dKO}$. Representative image from 50 cells imaged. (B) Pretreatment for 30 min with 0.1 mM dasatinib (Das.) prevents Syk(SH2)$^{SYFP2}$ recruitment. Representative image from 73 cells imaged. Quantification of Syk(SH2)$^{SYFP2}$ recruitment frequency is found in Supplemental Figure S1. Scale bars, 5 μm.

images of receptor aggregates and their corresponding Syk clusters at the adherent cell surface. From these images, we applied Bayesian multiple-emitter fitting (BAMF) (Fazel *et al.*, 2019) analysis to identify individual FcεRI aggregates and Syk clusters. BAMF has the advantage of accurately determining the fluorescence intensity of cytosolic nonclustered Syk-mNG and aggregated IgE-JF646 in our images, which improves the image segmentation used to generate aggregate masks and the calculation of signal within the mask (Supplemental Figure S4). From this segmented image, we determined the number of Syk clusters formed (Figure 4C) and the corresponding intensity of IgE-JF646 and Syk-mNG associated with individual aggregates (Figure 4D). We found a reduction in the total number of Syk clusters formed per cell when Lyn was absent (Figure 4C). In addition, individual FcεRI aggregates are less efficient at recruiting Syk in RBL-Lyn$^{KO}$ cells. The recruitment of Syk to receptor aggregates in RBL-WT cells has a linear correlation, as seen in Figure 4D. This is consistent with previous work showing that as FcεRI aggregates increase in intensity (i.e., receptor number), the amount of Syk-mNG recruited concomitantly increases (Schwartz *et al.*, 2017). In RBL-Lyn$^{KO}$ cells, the amount of Syk-mNG recruited to FcεRI aggregates of a specific intensity is consistently lower than that for RBL-WT cells (Figure 4D). Therefore, despite achieving robust degranulation, the reduced γ ITAM phosphorylation seen in RBL-Lyn$^{KO}$ cells (Figure 2) is translated to less efficient Syk recruitment (Figure 4D).

### Incomplete FcεRIγ ITAM phosphorylation supports Syk recruitment

Previous work has established that, by altering the pTyr profile of the FcεRI ITAMs, recruitment of accessory proteins, including Syk, Lyn, and SHIP1, can be modulated (Kimura *et al.*, 1996a; Furumoto *et al.*, 2004; Yamashita *et al.*, 2008). We previously showed that γ-subunits phosphorylated only at the C-terminal tyrosine are capable of recruiting Syk and propagating calcium signaling if the γ-subunits are preserved as physiological dimers (Travers *et al.*, 2019). The calcium release resulting from these monophosphorylated γ-subunits is delayed, however, similar to that of RBL-Lyn$^{KO}$ cells. We reasoned that the impaired Syk recruitment in RBL-Lyn$^{KO}$ cells may then be a result of incomplete γ-phosphorylation. To explore this possibility, we generated a double-knockout cell line deficient in Lyn and FcεRIγ (RBL-Lyn/γ$^{dKO}$ cells) using CRISPR-Cas9. FcεRI γ-subunits were reintroduced through transfection as either WT or single-tyrosine mutants (Y64F (FY), Y75F (YF)) or mutants lacking both tyrosines (Y64F-Y75F (FF)). The α- and β-subunits do not traffic to the plasma membrane without the γ-subunit, and therefore, IgE will not bind to RBL-Lyn/γ$^{dKO}$ cells. Confocal imaging showed successful integration of transfected FcεRIγ constructs into the receptor complex by restoration of fluorescent IgE binding (Figure 5 and Supplemental Figure S5). Expression of γ-WT led to successful recruitment of Syk-mNG to $DNP_{25}$-BSA cross-linked receptor aggregates (Supplemental Figure S5A). In contrast, γ-FF was not capable of Syk-mNG recruitment (Supplemental Figure S5B). When only the C-terminal tyrosine was present (γ-FY), Syk-mNG still clustered with receptor aggregates (Figure 5A and Supplemental Figure S1), whereas the N-terminal tyrosine alone (γ-YF) was not sufficient for Syk-mNG recruitment (Figure 5B and Supplemental Figure S1). Using the BAMF segmentation analysis described in Figure 4, we plotted the number of Syk clusters formed per cell over time in RBL-WT, Lyn$^{KO}$, and Lyn/γ$^{dKO}$(γ-FY) cells. Figure 5C confirms that the kinetics of Syk clustering is indeed delayed in the absence of Lyn. This delay in Syk recruitment is congruent with the observed delay in degranulation onset in RBL-Lyn$^{KO}$ cells (Supplemental Figure S6). RBL-Lyn/γ$^{dKO}$ cells expressing FcεRIγ-FY had Syk recruitment kinetics similar to that of RBL-Lyn$^{KO}$ cells (Figure 5C). These results support the idea that Syk is capable of interactions with incompletely phosphorylated γ ITAMs. Specifically, we demonstrate that the C-terminal tyrosine of the γ ITAM dimer becomes phosphorylated and is capable of recruiting Syk despite the absence of Lyn.

### Syk has productive interactions with both the γ and β ITAMs

To this point, our studies focused on Syk interactions with the γ ITAM. The role of the β ITAM serving as a platform to propagate Syk

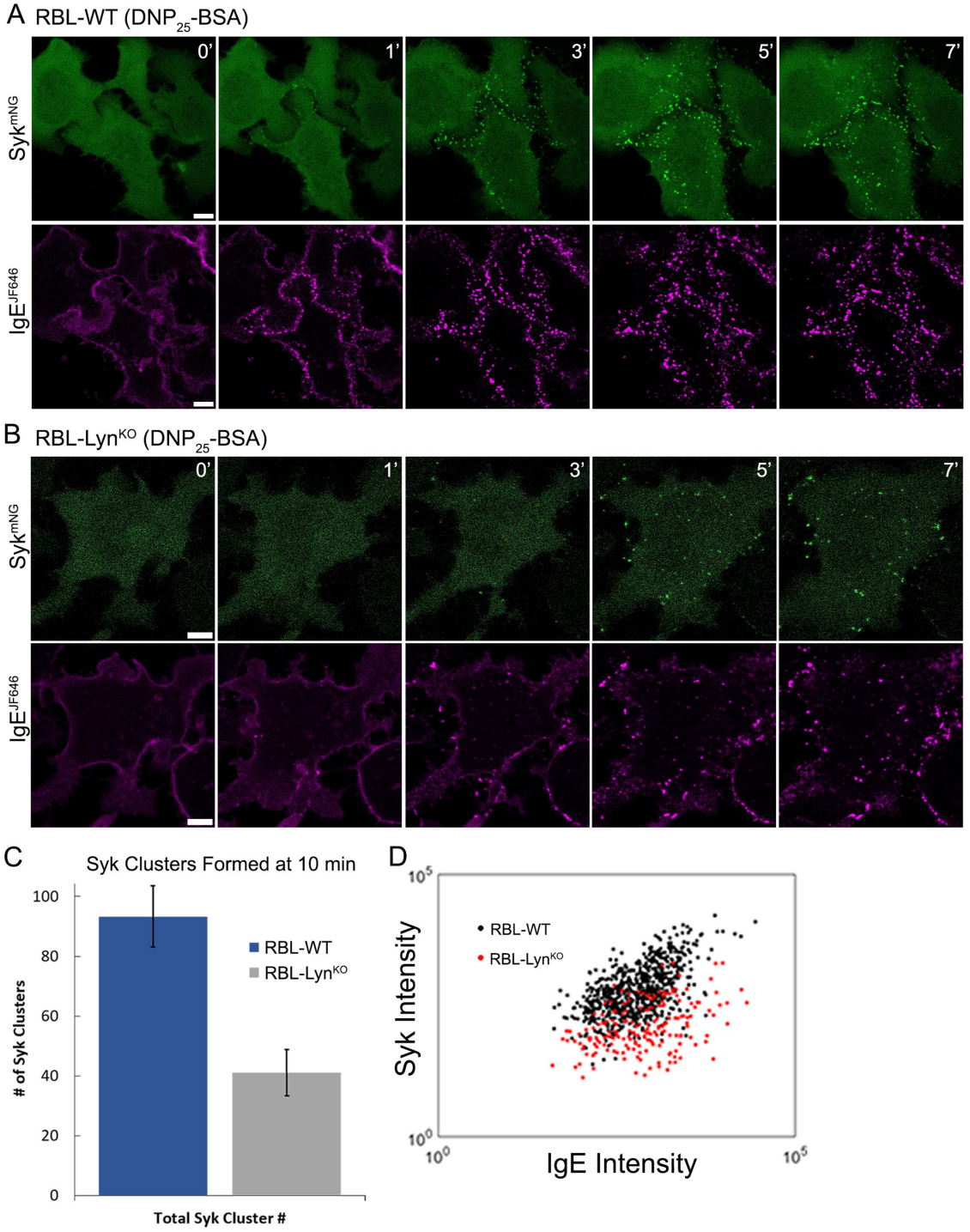


FIGURE 4: Syk recruitment is reduced in RBL-Lyn$^{KO}$ cells. (A) RBL-WT or (B) RBL-Lyn$^{KO}$ cells expressing Syk-mNG were cross-linked with 0.1 µg/ml $DNP_{25}$-BSA. Confocal images of IgE-JF646 aggregation and Syk recruitment were captured at specified time points after $DNP_{25}$-BSA addition. Scale bars, 5 µm. (C) Syk-mNG clustering was quantified from TIRF images captured at 10 min post–cross-linking. BAMF image analysis was used to identify and quantify the number of Syk clusters formed per cell. RBL-WT $n = 7$ cells, RBL-Lyn$^{KO}$ $n = 6$ cells. Values are mean ± SD. (D) Quantification of FcεRI aggregate capacity for Syk recruitment from the same images as in C. The FcεRI aggregate mask was defined by the IgE channel using BAMF, and the corresponding total intensity (arbitrary units) of IgE-JF646 and Syk-mNG within individual aggregates is plotted.

signaling has been suggested, but largely discounted (Wilson *et al.*, 1995; Furumoto *et al.*, 2004; Xiao *et al.*, 2005; Ra *et al.*, 2012). However, we had previously found that RBL-γ$^{KO}$ cells reconstituted with a γ-mutant lacking ITAM tyrosines (i.e., RBL-γ$^{KO}$(γ-FF)) are still capable of a weak calcium response (Travers *et al.*, 2019). We hypothesized that this signaling was due to the presence of the intact FcεRIβ ITAM, but separating the contributions of individual subunits is difficult when examining intact receptor. To determine whether Syk binds to

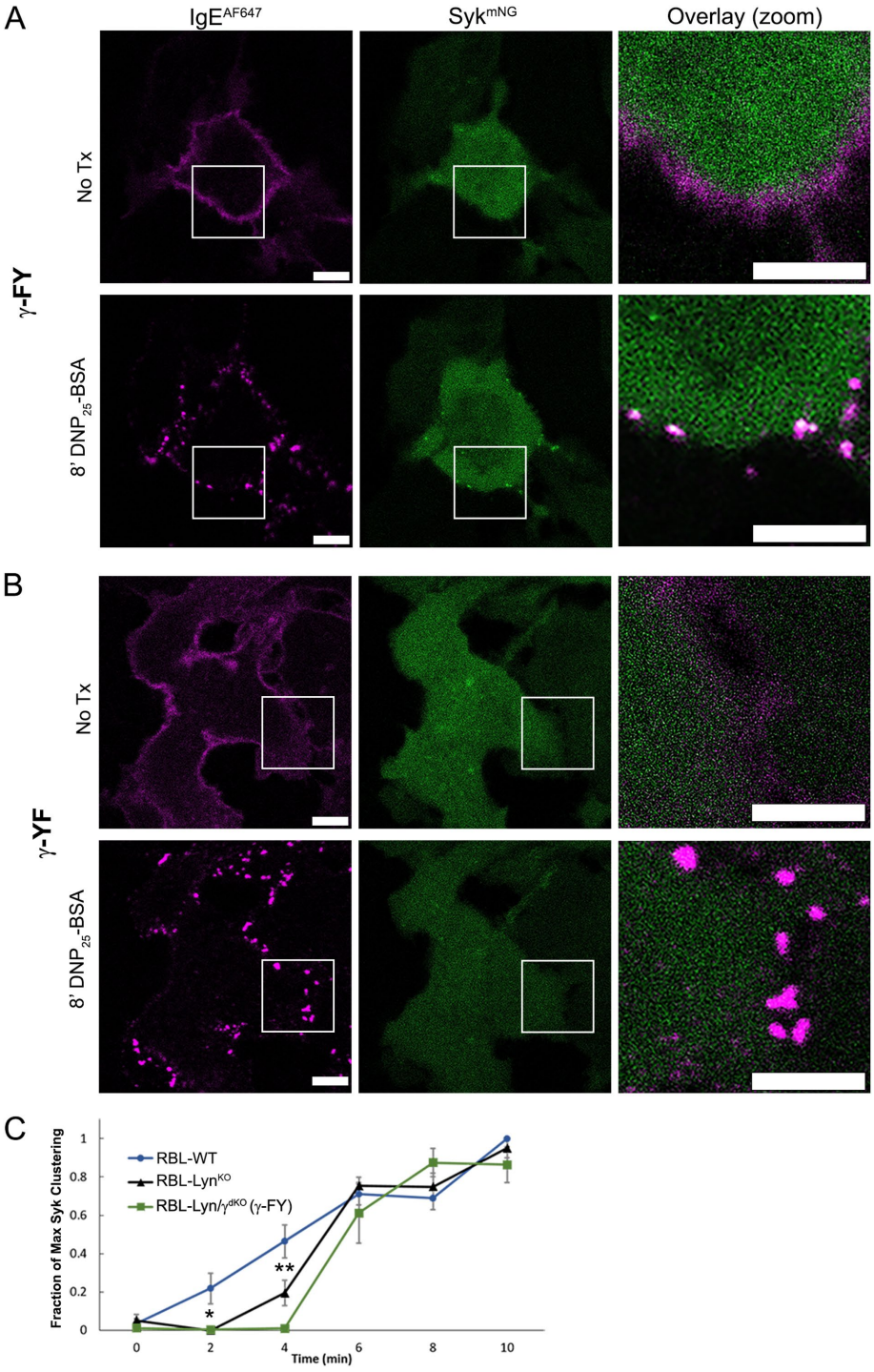


FIGURE 5: Weak Syk recruitment in RBL-Lyn$^{KO}$ cells is a result of incomplete FcεRIγ ITAM phosphorylation. (A, B) Confocal images of RBL-Lyn/γ$^{dKO}$ cells expressing both Syk-mNG (green) and an FcεRIγ mutant lacking either the N-terminal (γ-FY; A) or C-terminal (γ-YF; B) tyrosine. Cells were incubated overnight with IgE-AF647 (magenta) and activated with 0.1 μg/ml $DNP_{25}$-BSA. Recruitment of Syk-mNG was observed for cells expressing γ-FY ($n = 65$ cells) but not γ-YF ($n = 83$ cells). See also Supplemental Figure S1. Scale bars are 5 μm. (C) Quantification of Syk cluster formation over time. Time series of Syk-mNG clustering was acquired using TIRF. Each cell was normalized to its maximum cluster number; mean and SD of cluster values between cells; RBL-WT $n = 7$, RBL-Lyn$^{KO}$ $n = 5$, RBL-Lyn/γ$^{dKO}$(γ-FY) $n = 5$. * $P < 0.05$, ** $P < 0.01$, two-tailed ANOVA with Tukey's multiple comparison test. All other differences were nonsignificant.

the β ITAM, we used cells coexpressing Syk-mNG and chimeric Tac-Tac (TT)-γ or -β ITAM monomers. The TT constructs consist of the coding sequences of extracellular and transmembrane domains of the Tac antigen (IL2Rα, TT) fused with the γ- or β-subunit cytoplasmic tail sequence (Letourneur and Klausner, 1991; Wilson *et al.*, 1995; Travers *et al.*, 2019). Cells were first treated with an AF647-labeled anti-Tac antibody. This pretreatment generates quasi-dimers but does not activate signaling (Wilson *et al.*, 1995). Subsequent addition of an anti-mouse secondary antibody aggregates the TT-ITAMs and leads to phosphorylation and downstream signaling. As expected, aggregation of TT-γ resulted in Syk-mNG recruitment to the aggregates (Figure 6A and Supplemental Figure S1). Notably, we also observed Syk-mNG recruitment to aggregated TT-β (Figure 6B and Supplemental Figure S1).

Considering the weak calcium response of RBL-γ$^{KO}$ cells expressing a tyrosine-null γ-mutant (i.e., RBL-γ$^{KO}$(γ-FF)) (Travers *et al.*, 2019) and the ability of Syk to bind the β-subunit (Figure 6B), we revisited the possibility that the β-subunit can support signaling. We found that RBL-WT cells expressing TT-β are not capable of degranulation (Figure 6C), consistent with earlier work (Wilson *et al.*, 1995). However, while Syk is the critical positive signaling node for mast cells, a number of negative regulatory proteins are involved in balancing FcεRI signaling. We focused on SHIP1, which is a key player in setting the threshold for mast cell signaling and is a major "gatekeeper" of mast cell degranulation (Huber *et al.*, 1998; Mahajan *et al.*, 2014). SHIP1 contains a single SH2 domain that binds to phosphorylated ITAMs and an inositol 5′-phosphatase that regulates phosphoinositol levels. To remove SHIP1 regulation, we generated an RBL SHIP1 knockout cell line (RBL-SHIP1$^{KO}$), again using CRISPR-Cas9. We found that TT-β aggregation was able to induce degranulation in cells lacking SHIP1-negative regulation (Figure 6C). These data confirm that SHIP1 tightly regulates FcεRI signaling outcomes and suggest a direct role for SHIP1 in Syk regulation.

### Lyn is required for SHIP1 recruitment to FcεRI aggregates

We next considered that the ability of RBL-Lyn$^{KO}$ cells to support signaling, even though FcεRIγ ITAM phosphorylation and Syk recruitment are both reduced, could be a result of altered phosphatase engagement within the signalosome. Previous work

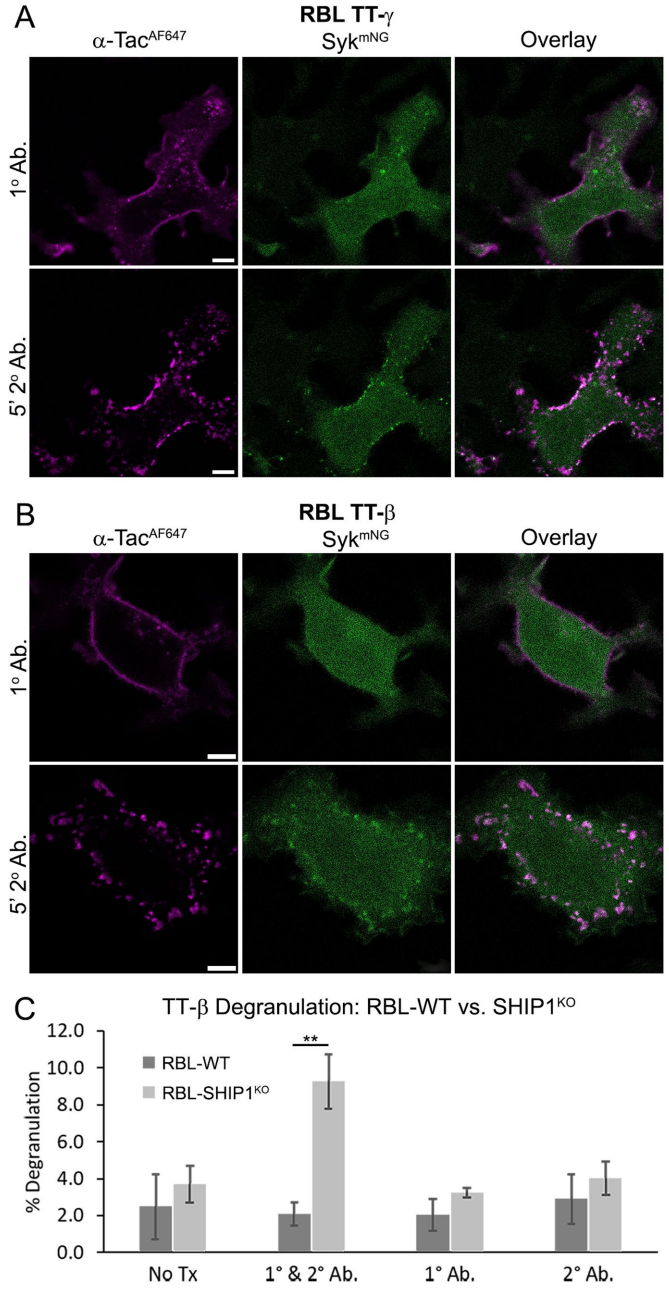


FIGURE 6: Functional Syk recruitment to the FcεRIβ ITAM. (A, B) RBL-WT cells coexpressing Syk-mNG (green) and (A) TT-γ or (B) TT-β. Cells are first labeled with AF647-conjugated anti-Tac primary antibody (magenta) followed by 5 min of large-scale cross-linking with 25 μg/ml anti-mouse secondary antibody. Syk-mNG recruitment is observed for both TT-γ and TT-β. Representative image shown from 60 (A) and 41 (B) cells imaged. See Supplemental Figure S1 for quantification of recruitment frequency. Scale bar is 5 μm. (C) RBL-WT and RBL-SHIP1$^{KO}$ cells were transfected to express the TT-β construct. Degranulation was quantified after cross-linking with 1 μg/ml TT-β anti-Tac antibody (1° Ab.) followed by anti-mouse antibody (2° Ab.). ** $P < 0.01$, paired two-tail $t$ test, $n = 9$.

indicated that SHIP1 activity is integrally tied to that of Lyn (Furumoto *et al.*, 2004; Mahajan *et al.*, 2014; Nunes de Miranda *et al.*, 2016), which led us to examine the efficiency of SHIP1 recruitment in RBL-Lyn$^{KO}$ cells. RBL-WT or -Lyn$^{KO}$ cells were transfected with SHIP1-mNG and incubated overnight with IgE-AF647. In RBL-WT cells, the recruitment of SHIP1-mNG to receptor aggregates is readily observed within 3 min of DNP$_{25}$-BSA cross-linking (Figure 7A and Supplemental Figure S1). In contrast, SHIP1-mNG recruitment to receptor aggregates is not observed in RBL-Lyn$^{KO}$ cells (Figure 7B and Supplemental Figure S1). The inability of FcεRI to recruit SHIP1 in these cells suggested that the required tyrosines for docking are not phosphorylated. Others have specifically tied the phosphorylation of the β ITAM to SHIP1 recruitment (Furumoto *et al.*, 2004; Xiao *et al.*, 2005). We confirmed this finding using the chimeric TT-ITAMs. Figure 7, C and D, shows that SHIP1 is indeed recruited to TT-β after aggregation, but not TT-γ. Because SHIP1 recruitment is specific to the β ITAM, the loss of SHIP1 recruitment indicates that the β ITAM is not phosphorylated in RBL-Lyn$^{KO}$ cells. Therefore, while γ ITAM phosphorylation is initiated by another compensating kinase and amplified by Syk, β ITAM phosphorylation requires Lyn. Furthermore, the loss of SHIP1 recruitment indicates that the negative regulatory mechanisms in RBL-Lyn$^{KO}$ cells are inherently reduced.

### SHIP1 limits Syk residency time at the receptor

While the loss of SHIP1 might explain how weak Syk recruitment propagates signaling in RBL-Lyn$^{KO}$ cells, the mechanism through which SHIP1 regulates Syk behavior was still not clear. We used single particle tracking (SPT) to determine whether the presence of SHIP1 influences the formation of the FcεRI signalosome. In previous work, we described the use of SPT to track Syk-mNG membrane recruitment and quantify the lifetime of FcεRI:Syk interactions (Schwartz *et al.*, 2017). Briefly, RBL cells expressing Syk-mNG were imaged using TIRF microscopy such that Syk-mNG trajectories are captured only when the molecule enters the TIRF field and slows in mobility as it interacts at the plasma membrane (Supplemental Video 1). The track length of Syk-mNG trajectories is then a readout of the binding lifetime of individual Syk-mNG molecules at the cell membrane. By fitting the population of Syk-mNG trajectories, we are able to extract the off-rate of Syk interactions with FcεRI, where the off-rate is the inverse of the binding lifetime (Schwartz *et al.*, 2017). We used this SPT approach to measure Syk dynamics in the presence or absence of SHIP1. Figure 8A shows that the distribution of Syk-mNG track lengths shifts to longer values upon DNP$_{25}$-BSA cross-linking. This is consistent with an increase in Syk recruitment to the membrane upon FcεRI activation. We fitted these distributions using our previously described two-component model, where the slow off-rate ($k_s$) corresponds to long-lived Syk interactions with phosphorylated FcεRI and the fast off-rate ($k_f$) signifies nonspecific interactions of Syk with the membrane. We first examined Syk-mNG recruitment in the presence of SHIP1 and found off-rates consistent with those reported in Schwartz *et al.* (2017), with $k_s = 0.527\ s^{-1} \pm 0.040$ and $k_f = 1.6445 \pm 0.095$ (Figure 8B). Addition of DNP$_{25}$-BSA caused an increase in the fraction of the slow component ($\alpha_s$), from $0.078 \pm 0.024$ when unstimulated to $0.161 \pm 0.022$ with receptor cross-linking (Figure 8C). This increase in the fraction of $\alpha_s$ is consistent with an increase in Syk recruitment after FcεRI activation. As seen in Figure 8A, the distribution of Syk-mNG track lengths in RBL-SHIP$^{KO}$ cells also shifted to longer time values after FcεRI activation. Interestingly, the distribution in nontreated RBL-SHIP$^{KO}$ cells is more similar to that of activated RBL-WT cells. Fitting these distributions revealed that the off-rate for $k_s$ is reduced in RBL-SHIP$^{KO}$ ($k_s = 0.323\ s^{-1} \pm 0.004$), such that the absence of SHIP1 allows for longer-lived interactions of Syk with FcεRI (Figure 8B). Consistent with the right-shifted track length distributions (Figure 8A), we found that the fraction of long-lived Syk events at the membrane is higher in RBL-SHIP1$^{KO}$ cells, for resting and activated cells (Figure 8C). These results reveal that SHIP1 regulates both the amount and duration of Syk binding to FcεRI. An increase in membrane-resident Syk in cells

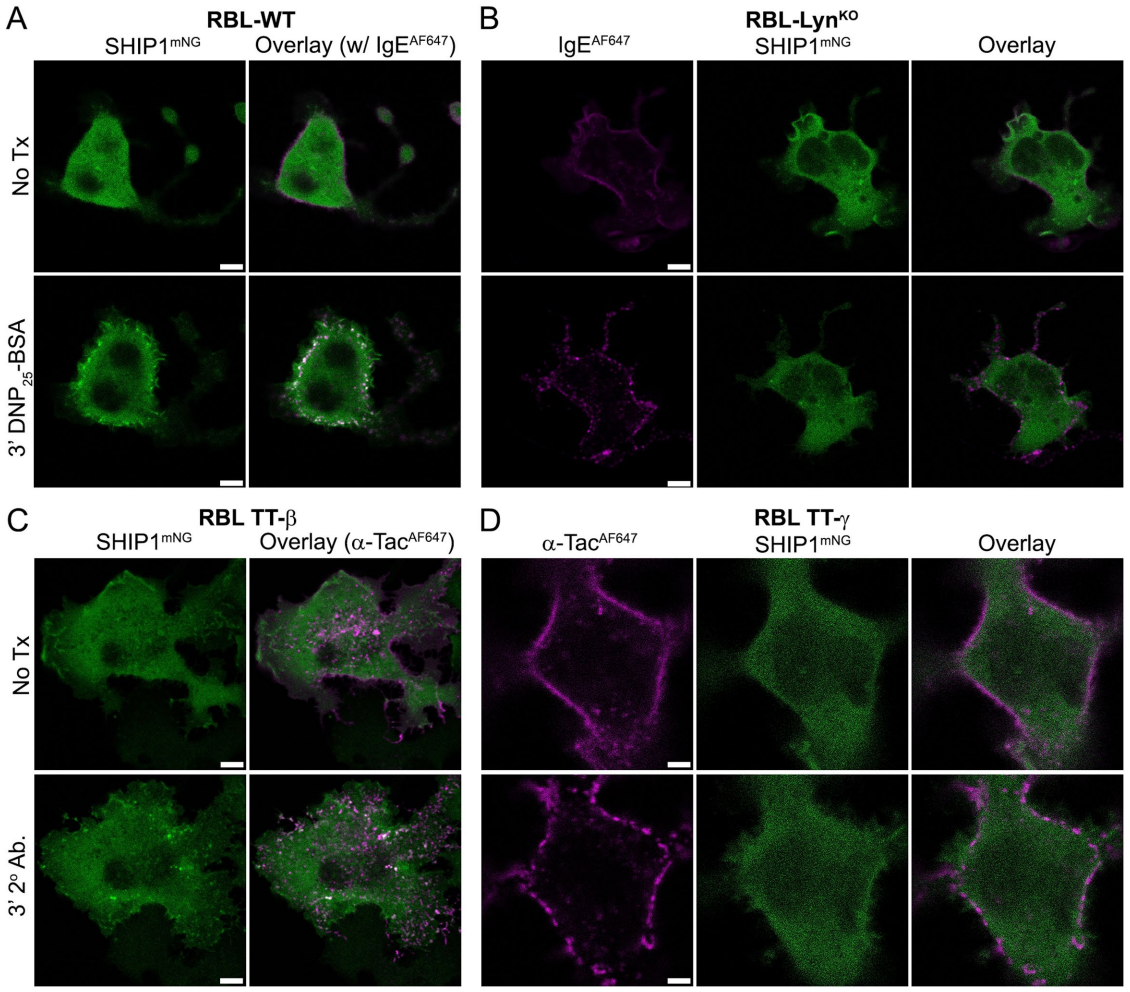


**FIGURE 7:** SHIP1 recruitment is absent in RBL-Lyn$^{KO}$ cells. (A) RBL-WT or (B) Lyn$^{KO}$ cells were transfected to express SHIP1-mNG (green) and incubated overnight with IgE-AF647 (magenta). Cells were activated with the addition of 0.1 µg/ml $DNP_{25}$-BSA and confocal images collected at specified time points. SHIP1-mNG recruitment is not observed in the absence of Lyn. (C, D) RBL-WT cells coexpressing SHIP1-mNG (green) and either (C) TT-β or (D) TT-γ. Aggregation of the anti-Tac primary antibody (magenta), with 25 µg/ml anti-mouse secondary antibody, induced SHIP1-mNG recruitment to TT-β but not TT-γ. Representative image shown of 103 (A), 107 (B), 59 (C), and 38 (D) cells imaged. See Supplemental Figure S1 for quantification of SHIP1-mNG recruitment frequency. Scale bar is 5 µm.

lacking SHIP1 suggests that the regulatory behavior of SHIP1 acts independent of receptor cross-linking and plays a role in preventing aberrant, constitutive FcεRI signaling. The idea that SHIP1 acts to prevent aberrant signaling is supported by previous work showing that even in the resting state phospho-SHIP1 is present at the cell membrane in RBL cells (Mahajan *et al.*, 2014). The longer Syk residency time at the receptor when SHIP1 is absent may be the mechanism that facilitates Syk amplification of γ-subunit ITAM phosphorylation in RBL-Lyn$^{KO}$ cells. In previous work, we found that an increase in off-rate, meaning a more transient interaction, led to a reduction in Syk phosphorylation and signaling outcomes (Schwartz *et al.*, 2017). To determine whether the decrease in FcεRI:Syk off-rate observed here has an impact on Syk function, we compared phosphorylation of Syk and LAT by Western blot analysis. The kinetics and extent of phosphorylation were increased for both Syk and LAT when SHIP1 was knocked out (Figure 8, D and E).

## DISCUSSION

A cell's signaling response is determined by the culmination of activities from both positive- and negative-signaling molecules. This balance is particularly critical in mast cell signaling, where cellular secretory responses depend on the formation of FcεRI aggregates capable of overriding negative regulatory signals (Mendoza and Minagawa, 1982; Kovářová *et al.*, 2001; Young *et al.*, 2003). We investigated the contribution of ITAM pTyr patterns, along with the roles of Lyn, Syk, and SHIP1 in the building of the FcεRI signalosome. We began by defining the signaling profile of RBL-Lyn$^{KO}$ cells and showed that, despite lacking Lyn and Fyn, calcium release and degranulation readily occurred after $DNP_{25}$-BSA antigen cross-linking. We did note a delay in the timing of both responses, which was linked to slower and less efficient Syk recruitment. These delays in RBL-Lyn$^{KO}$ cell outcomes are similar to the delay in calcium release (Nishizumi and Yamamoto, 1997; Parravicini *et al.*, 2002) and degranulation (Hernandez-Hansen *et al.*, 2004) observed in Lyn-deficient murine bone marrow mast cells (BMMCs). However, BMMCs express Fyn, which was shown to compensate for the absence of Lyn (Parravicini *et al.*, 2002; Hernandez-Hansen *et al.*, 2004; Fasbender *et al.*, 2017). Studies of BCR signaling in Lyn-deficient B-cells have also reported a delay in Syk and Ig-α phosphorylation, as well as calcium release (Takata *et al.*, 1994; Yanagi *et al.*, 1996;

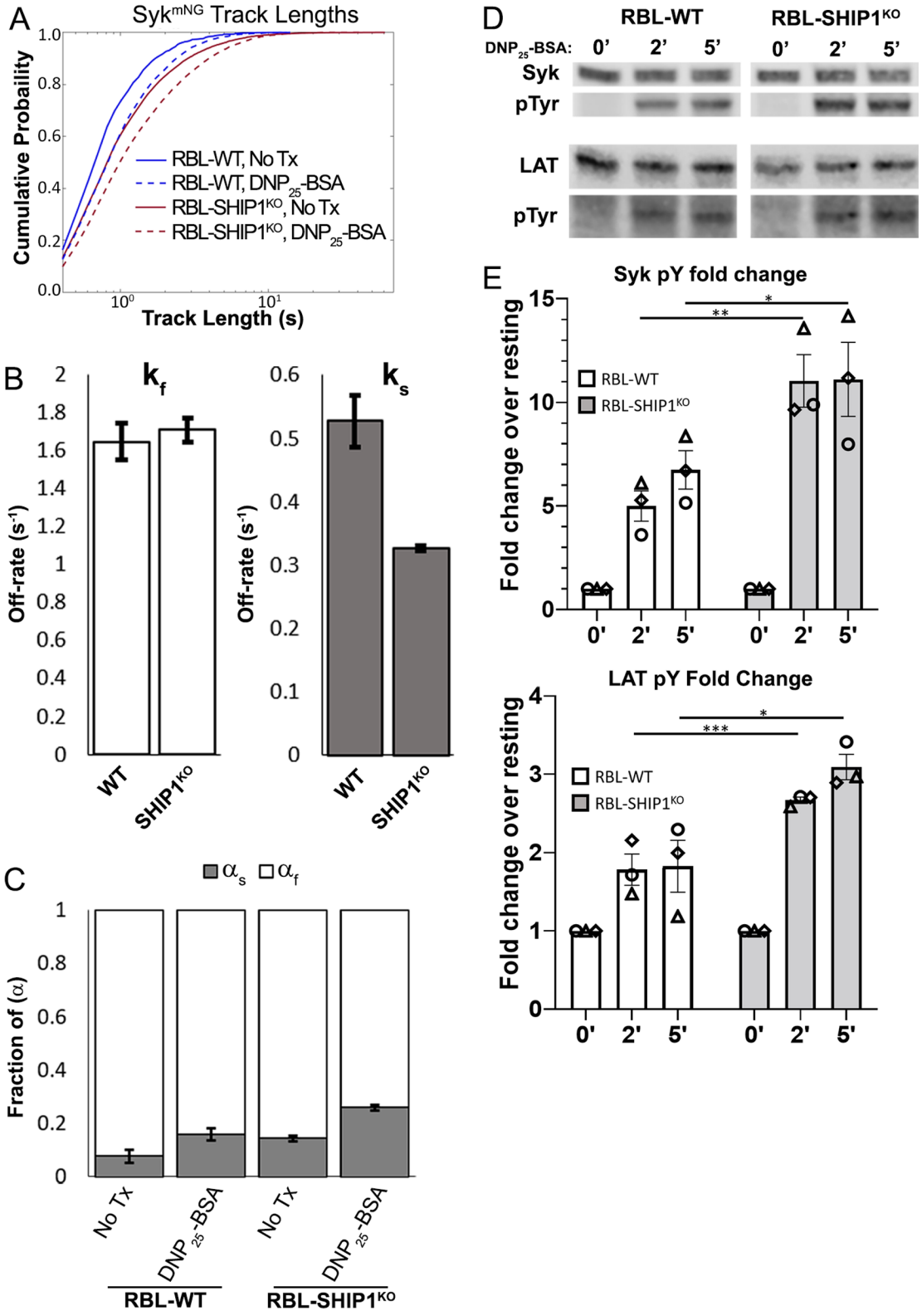


FIGURE 8: SHIP1 acts to reduce Syk binding duration and activity at the plasma membrane. (A) Cumulative probability distributions of trajectory lengths (membrane residency time) for Syk-mNG before (solid lines) and 1–5 min after (dashed lines) addition of 0.1 µg/ml $DNP_{25}$-BSA, for RBL-WT (blue) and RBL-SHIP1$^{KO}$ (red) cells. Number of trajectories (*n*): No Tx WT $n = 1040$, +DNP-BSA WT $n = 5129$, No Tx SHIP1$^{KO}$ $n = 8071$, +DNP-BSA SHIP1$^{KO}$ $n = 15661$. Data collected from at least 20 cells per condition over 3 d. (B) The fast ($k_f$) and slow ($k_s$) off-rates calculated for Syk-FcεRI interactions in each cell type. (C) The fraction of slow ($\alpha_s$) and fast ($\alpha_f$) Syk-mNG interactions both before and after $DNP_{25}$-BSA cross-linking. Values in B and C are from fitting of data in A as described in *Materials and Methods*. Error bars are a 68% credible

Chan *et al.*, 1997). The observation that B-cells lacking Lyn can support ITAM phosphorylation led to the hypothesis that Syk itself plays a role in directly phosphorylating ITAMs. Several studies have demonstrated that Syk is capable of phosphorylating the C-terminal tyrosine of the BCR (Nishizumi *et al.*, 1995; Pao and Cambier, 1997; Li *et al.*, 1999; Kawakami *et al.*, 2000; Ma *et al.*, 2001; Rolli *et al.*, 2002). In addition, mathematical modeling reinforced the importance of BCR clustering to initiate SFK-independent Syk activity (Mukherjee *et al.*, 2013), suggesting that a specific threshold of Syk recruitment is required for Syk to begin phosphorylating receptor ITAMs. We found that the γ ITAM is a substrate for Syk kinase activity. However, we also show that Syk cannot bind to unphosphorylated FcεRI so that SFK activity is required to first phosphorylate the ITAM and initiate Syk recruitment. In the absence of Lyn only low-level γ-phosphorylation is achieved, but this is sufficient to promote Syk binding and facilitate Syk amplification of γ-phosphorylation in a positive feedforward manner.

Prior work using mass spectrometry analysis has shown that γ ITAM phosphorylation is not complete even under optimal signaling conditions (Yamashita *et al.*, 2008). Furthermore, Syk is instrumental in a broad range of immunoreceptor signaling cascades, across several cell types. Therefore, we leveraged the FcεRI phosphorylation model in RBL-Lyn$^{KO}$ cells to understand critical attributes of the Syk kinase such as its docking capacity to adapt to different ITAM phosphorylation patterns and under what conditions productive signaling is supported. We showed that the C-terminal tyrosines of the γ-dimer are necessary and sufficient for Syk recruitment, supporting the ability of Syk to bind in *trans*. The possibility of this noncanonical *trans* conformation was predicted by molecular dynamics modeling and confirmed using mutagenesis of the γ ITAMs (Travers *et al.*, 2019). This previous work also showed that two pTyr are required to functionally engage Syk because the single-tyrosine γ-FY mutant could signal when in a physiologically relevant dimer structure, but not when presented as TT-γ constructs (Travers *et al.*, 2019). Thus, Syk must bridge across the γ-dimer to engage two pTyr in a *trans* binding orientation. While this provides an alternative mode of signaling under conditions of incomplete ITAM phosphorylation, it suggests that only one Syk can bind in *trans* to a γ-dimer compared with the two Syk molecules that can simultaneously bind in *cis* to a fully phosphorylated γ-dimer (Travers *et al.*, 2019). This limited Syk binding capacity is consistent with the reduced Syk recruitment found in RBL-Lyn$^{KO}$ cells. The delay in Syk activity in RBL-Lyn$^{KO}$ cells also raises the possibility that the kinase compensating for Lyn may only be able to phosphorylate the C-terminal tyrosines of the γ ITAM. Alternatively, the interactions of the Syk-SH2 domains with the N-terminal pTyr may be too weak to support *trans* bridging, as has been previously reported (Yamashita *et al.*, 2008). Nevertheless, the reduced Syk recruitment to monophosphorylated γ-chains supports the idea that Lyn acts to accelerate signaling through its more efficient kinase activity (Hibbs *et al.*, 1995; Nishizumi *et al.*, 1995; Chan *et al.*, 1997; Hernandez-Hansen *et al.*, 2004). The potential for Syk to bind ITAMs in *trans* also contributes to our understanding of hemITAM:Syk interactions. Because hemITAMs contain a single tyrosine, they cannot support Syk binding in *cis* and rely on the proper receptor spacing to bring two pTyr in sufficient proximity for *trans* Syk docking (Watson *et al.*, 2009; Bauer *et al.*, 2017; Bauer and Steinle, 2017). Work in hemITAMs combined with our findings using single-tyrosine mutant γ ITAMs suggests a degree of overlap in the models for how Syk docks to both γ ITAM and hemITAM dimers. The flexibility of Syk binding conformations is likely related to its role as a critical node for multiple immunoreceptor signaling networks.

In addition to noncanonical Syk:γ binding, we showed that Syk undergoes productive interactions with the β ITAM. The β ITAM is well-known for its interactions with Lyn and recruitment of negative signaling proteins, including SHIP1 (Furumoto *et al.*, 2004; Xiao *et al.*, 2005). We found that Syk is also readily recruited to TT-β. A role for β:Syk binding was unclear, with previous work failing to show Syk:β interactions by coimmunoprecipitation and indications that TT-β signaling alone does not induce degranulation (Wilson *et al.*, 1995; Furumoto *et al.*, 2004). However, we found that removal of SHIP1 allows for TT-β aggregation to induce degranulation. This result highlights the careful controls that are in place to regulate ITAM-based signaling.

SHIP1 was not recruited to the FcεRI signalosome in RBL-Lyn$^{KO}$ cells, indicating that the required tyrosine for docking was not phosphorylated. We examined this using the chimeric TT-ITAMs where SHIP1 is recruited to TT-β but not TT-γ. Because SHIP1 recruitment is specific to the β ITAM, the loss of SHIP1 binding indicates that the β ITAM is not phosphorylated in RBL-Lyn$^{KO}$ cells. Therefore, while γ ITAM phosphorylation is initiated by another compensating kinase and further increased by Syk, β ITAM phosphorylation requires Lyn. Because SHIP1 is not recruited to FcεRI aggregates in RBL-Lyn$^{KO}$ cells, the negative regulation is naturally reduced in these cells. We postulated that the absence of SHIP1 permits the low-level Syk recruitment and γ ITAM pTyr levels observed in RBL-Lyn$^{KO}$ cells to propagate signaling to the point of degranulation. Because SHIP1 contains an SH2 domain that binds to phosphorylated ITAMs, the mechanism that leads to its gatekeeper role could be based on competitive binding to ITAMs with Syk. A competitive mechanism has been suggested for controlling anergy in B-cells where SHIP1 and Syk are both shown to bind to the same BCR ITAM subunits (O'Neill *et al.*, 2011). Anergic B-cells were found to have a high level of phospho-SHIP1, and the loss of SHIP1 resulted in a loss of B-cell anergy. Our observation that SHIP1 is recruited only to the β ITAM of FcεRI reduces the likelihood of competitive ITAM binding as the key mechanism because the γ ITAM alone can support Syk recruitment and signaling. Alternatively, the lipid environment may play a role in Syk regulation. Park *et al.* (2016) found that ZAP-70 binds to both PI(3,4,5)$P_3$ (PIP$_3$) and PI(4,5)$P_2$, with higher affinity for PIP$_3$, through "alternate cationic patches" (ACPs). ACPs are located outside of the pTyr binding pocket of the C-terminal SH2 domain, allowing for simultaneous binding of ZAP-70 to ITAM pTyr and PIP$_3$, with PIP$_3$ possibly acting to stabilize ZAP-70 at the plasma membrane. They also found that a similar interaction exists between PIP$_3$ and the Syk C-terminal SH2 domain. Because SHIP1 is a lipid phosphatase that converts PIP$_3$ to PI(3,4)$P_2$, we predicted that SHIP1 might act to destabilize Syk membrane localization by reducing the PIP$_3$ available for ACP binding. Indeed, our SPT measurements

interval. (D) Representative immunoblot of Syk and LAT phosphorylation in RBL-WT or SHIP1$^{KO}$ cells. Cells were treated with 0.1 µg/ml DNP$_{25}$-BSA for the indicated time points and probed for total protein and phosphorylation of Syk (top) and LAT (bottom). Three independent experiments were performed. (E) Quantification of Western blots as described in D for Syk (top plot) and LAT (bottom plot) phosphorylation, *** $P < 0.001$, ** $P < 0.01$, * $P < 0.05$. ANOVA with Šídák's multiple comparison test. Bar graphs display average values ± SD from three independent experiments, and matching symbols indicate results from the same individual experiment.

revealed that the interaction between Syk and FcεRI is longer-lived in RBL-SHIP1$^{KO}$ cells. While this result is consistent with the hypothesis that PIP levels can alter Syk lifetime at the membrane, more work is needed to confirm this mechanism. Importantly, we found that the reduction in Syk off-rate was translated into increased phosphorylation of both Syk and LAT. In previous work, we showed that small changes in Syk binding kinetics modulated mast cell signaling outcomes, albeit in that case we found the reciprocal outcome where an increase in off-rate resulted in a reduction of Syk phosphorylation and signaling (Schwartz *et al.*, 2017). Together these studies show a direct correlation between FcεRI:Syk binding lifetime and Syk function, further supporting the idea that the timing of protein–protein interactions is finely tuned to optimize protein modification.

Our study has revealed several unanticipated ways that FcεRI signaling is regulated. The flexibility of ITAM-based signaling is demonstrated in the ability of Syk to take advantage of incomplete γ-phosphorylation and directly drive positive signaling. Furthermore, noncanonical Syk binding, either through β ITAM binding or *trans* γ ITAM bridging, can propagate signaling. Here, we were able to overcome the inhibitory signaling axis by removal of only a single component of negative signaling. While positive signaling is allowed to propagate with SHIP1 knocked out, the signaling outcomes were still dampened, as would be expected when multiple negative regulators are involved. Determining the spatiotemporal relationships for other FcεRI recruited phosphatases, such as SHP1 and SHP2 (Furumoto *et al.*, 2004; Mahajan *et al.*, 2014), would provide further insight into how inhibitory signals are orchestrated to maintain control on positive signals. The identification of a novel regulatory role where SHIP1 acts to modulate the interaction time between Syk and FcεRI supports the idea that signaling is also sensitive to the duration of protein–protein interactions. Taking the results together, this work highlights the ability of ITAM-based signaling to respond to various ITAM phosphorylation patterns, Syk binding conformations, and the presence/absence of key regulatory molecules. These molecular mechanisms are likely applicable across the different MIRR systems and provide insight into how disparate immunoreceptors can utilize conserved signaling cascades to tailor their cellular outcomes.

## MATERIALS AND METHODS

Request a protocol through *Bio-protocol*.

### Reagents

MEM was purchased from Life Technologies (Grand Island, NY). AlexaFlour647 (AF647)-labeled anti-Tac IgG was from BioLegend (San Diego, CA), and anti-mouse IgG was from Jackson ImmunoResearch Laboratories (West Grove, PA). Fura-2AM was from Molecular Probes (Eugene, OR). $DNP_{25}$-BSA was from Thermo Fisher Scientific (Waltham, MA; catalogue #A23018), and anti-DNP-IgE was affinity purified from ascites (Covance, Denver, PA) according to the methods of Liu *et al.* (1980). AF647-labeled IgE was prepared using AlexaFluor647 NHS Ester (succinimidyl ester; Thermo Fisher Scientific). Janelia Fluor 646–labeled IgE (JF646) was prepared using Janelia Fluor 646 NHS Ester (Janelia Fluor 646 succinimidyl ester, Tocris; 6148). Antibodies used are as follows: anti-pY (4G10) was a gift from J. Cambier, (University of Colorado) anti–mouse-horseradish peroxidase (HRP) (Cell Signaling Technology; 7076S) and anti–rabbit-HRP secondary (Santa Cruz; sc-2004), Lyn (Abcam; ab71093), Src (Cell Signaling Technology; 2110), Lck (Antibodies-Online; ABIN4965391), Yes1 (R&D Systems; AF3205); Fyn (R&D Systems; MAB3574), SHIP1 (Santa Cruz; sc-136066), vinculin (Santa Cruz; sc-7F9), β-actin (Sigma; A2668), FcεRIγ (EMD Millipore; 06-727), goat anti-rat IgE (Abnova; PAB29749).

### Cell culture

RBL-2H3 cells were cultured in MEM supplemented with 10% heat-inactivated fetal bovine serum, 1% penicillin/streptomycin, and 1% L-glutamine (Metzger *et al.*, 1986; Wilson *et al.*, 2000). To ensure cell functionally, IgE binding and degranulation response was recorded after each thaw and used for up to 10 passages. Transfections were performed using the Amaxa system (Lonza) with Solution L and Program T-20. Stable cell lines were generated through G418 selection over a 1-wk period followed by isolation of positive, mNG-expressing cells using an iCyt cell sorter with a 525/50 nm emission filter. Cell lines were checked for equal expression levels before experiments using an Accuri C6 Plus cytometer (BD Biosciences) and sorted as needed. For all microscopy experiments, cells were plated into eight-well Lab-Tek (Nunc) chambers at a density of $4 \times 10^4$ cells/well, or a six-well tissue culture plate (Fablab) on round cover glass, #1.5 thickness, 25 mm (Warner Instruments) at a density of $2 \times 10^5$ cells/well, primed overnight with 1 μg/ml IgE, and imaged within 24 h.

### Plasmid constructs

Syk-mNG referred to murine Syk DNA, SHIP1-mNG referred to human SHIP1 DNA, Src-GFP referred to murine Src DNA, Lck-GFP referred to murine Lck DNA, and FcεRIγ referred to rat FcεRIγ DNA. For mNG constructs, they consisted of the respective DNA being fused to mNG via a short V5 linker (GGTAAGCCTATCCCTAACCCTCTCCTCGGTCTCGA TTCTACG) tag. The V5 tag was added to mNG (Allele Biotechnology User License) via fusion PCR. Fusion to V5-mNG was generated by gene fusion PCR using PfuUltra DNA polymerase (Stratagene) (Ho *et al.*, 1989). Total cDNA was amplified by PCR before subcloning into the pcDNA3.1 directional topo vector (Life Technologies). Constructs used for reconstitution of FcεRIγ WT and mutants in FcεRIγ$^{KO}$ cells were prepared in the pcDNA3.1 vector (Invitrogen). The Lck-GFP construct was purchased from OriGene Technologies (Origene; MG226723). Src-EGFP was a gift from Mainou and Dermody (2011), Vanderbilt University (Addgene plasmid #110496; http://n2t.net/addgene:110496; RRID:Addgene_110496).

The Syk(SH2)-SYFP2 construct was truncated after amino acid 263 of Syk (to not include the interdomain B or the kinase domain). The SYFP2 (iGEM BBa_K864100) gene was amplified with primers containing *Age*I and STOP-STOP-*Xho*I sequences and was expressed after the N-terminal part of Syk after a short linker sequence (GCGGCCGGTCTGGCCCATATGGGAGGCGGTGGGTCTGGTGGCGGTGGCAGCACCGGT). The construct was prepared in the pcDNA3.1 vector.

Chimeric TT-γ receptors have been described previously (Letourneur and Klausner, 1991). Constructs for reconstitution of FcεRIγ WT and mutant γ in FcεRIγ$^{KO}$ cells were prepared in the pcDNA3.1 vector (Invitrogen) (Travers *et al.*, 2019).

### Genome editing

Cas9-mediated DNA cleavage was used to knock out the endogenous gene coding for each respective protein in RBL-2H3 cells via the insertion of a premature stop codon in the first exon of the respective gene. A highly specific single guide RNA (gRNA) targeting either the first exon of rat Lyn (5′-TGAAAGACAAGTCGTCTGGG-3′), Syk (5′-GGCCAGAGCCGCAATTACCT-3′), SHIP1 (5′-AGGTCGTGGGCGAAGGCCTG-3′), or FcεRIγ (5′-GCAAGAACAAGATCACCGCT-3′) was designed using the http://crispr.mit.edu portal and then subcloned into the PX458 vector (Addgene plasmid #48138) for simultaneous expression of the gRNA, WT Cas9, and a green

fluorescent protein (GFP) reporter. For the gRNA subcloning, two partially complementary oligonucleotides (Integrated DNA Technologies) were assembled by PCR. Gel-purified PCR products were cloned into *Bbs*I-digested PX458 using Gibson Assembly (NEB) following the manufacturer's specifications. After cloning and sequencing, the final plasmid was used to transiently transfect RBL-2H3 cells with the Amaxa system (Lonza) using Solution L and Program T-020. Positive, GFP-expressing cells were selected by flow cytometry using an iCyt cell sorter and immediately plated at a single cell density in 96-well plates. Subclones were screened using immunoblotting to identify clones with successful knockout of the respective protein, confirmed with at least two independent sample preparations. Cells were monitored for proper cell growth and morphology, and degranulation and calcium assays were used to verify cell line functionality. Appropriate FcεRI surface expression was confirmed by fluorescent IgE binding and quantified by flow cytometry analysis, with the exception of the γ-knockout lines, which were confirmed by the absence of fluorescent IgE binding. The absence of residual GFP expression in knockout clones was assessed using a Nikon TE2000 epifluorescence microscope.

### Fura-2AM calcium assay

In all cases, cells were washed with buffer and incubated in 2 µM Fura-2AM buffer for 20 min at room temperature (RT) followed by an additional buffer wash. Ratio images were acquired at 35°C using an Olympus IX71 inverted microscope outfitted with a UPLANSAPO 60X/NA1.2 water emersion objective coupled to an objective heater (Bioptechs). Cells were activated by cross-linking with $DNP_{25}$-BSA, added at 30 s during a total of 5 min of imaging. Ratiometric changes in cytosolic calcium were determined by alternating between 340 and 380 nm at 1 Hz with a xenon arc lamp monochromator (Cairn Research OptoScan) and collecting the interleaved Fura-2 fluorescence emissions at 510 nm with an iXon 887 electron-multiplying charge-coupled device (EMCCD) camera using IQ3 imaging software (Andor Technology). Offline ratiometric analysis was performed over time with a custom MATLAB script for each cell (15–20 per field of view) to assess calcium release.

### Degranulation assay

Cells were grown in 24-well tissue culture plates for 24 h and primed with 1 µg/ml IgE overnight, except for TT antibody cross-linked cells. For TT degranulation assay, cells were incubated for 10 min with primary antibody (anti-Tac-AF647) before washes and cross-linking with secondary antibody. Cells were stimulated in Hank's buffer with the indicated concentration of $DNP_{25}$-BSA or the respective antibody for 30 min at 37°C. Release of granular content was measured by β-hexosaminidase concentration as previously described (Schwartz *et al.*, 2017).

### Confocal microscopy and imaging

Confocal images were obtained using a Leica DMi8 inverted microscope. A Leica Harmonic Compound PL apochromatic CS2 63X water objective with a correction collar (1.2 NA) was used for imaging. A tunable white light laser (470–670 nm) using 3% laser power and 488 nm (i.e., mNG excitation), 514 nm (i.e., SYFP2 excitation), or 633 nm (i.e., AF647 or JF646 excitation) notch filters for excitation. Images were 1024 × 1024 pixels and were acquired at a scan speed of 400. Two hybrid detectors collected photons at 500–540 nm (mNG collection) or 520–560 nm (SYFP2 collection) for green and 650–700 nm for far-red channels on the standard mode setting. Live cells were imaged at 35°C with temperature maintained using a Bioptics objective heater.

### SPT and lifetime analysis and microscopy optical setup

TIRF imaging data were collected using an inverted microscope (IX71; Olympus) equipped with a 150×/1.45 NA oil-immersion, TIRF objective (U-APO; Olympus). A 637-nm laser diode (HL63133DG; Thorlabs) was used for AF647 excitation, and a 488-nm laser (Cyan Scientific; Spectra-Physics) was used for fluorescence excitation of mNG. A quad-band dichroic and emission filter set (LF405/488/561/635-A; Semrock) was used for sample illumination and emission. Emission light was separated onto different quadrants of an EMCCD camera (iXon 897; Andor Technologies), using a custom-built two-channel splitter with a 655-nm dichroic (Semrock) and 584/20-nm and 690/20-nm additional emission filters. Images had a pixel size of 0.106 µm and were acquired at 10 frames/second (100 ms exposure time).

The analysis algorithms and parameters used to track individual mNG molecules were previously described in Schwartz *et al.* (2017). Briefly, tracks were analyzed using home-built MATLAB code that localized single particles per frame and determined connections between frames. The collected tracks were fitted to a two-component distribution to determine the off-rates of Syk at the membrane (Schwartz *et al.*, 2017).

### Localization intensity–based change point detection and thresholding

As previously described by Schwartz *et al.* (2017), single tracks that were represented by more than a single particle within a diffraction-limited area were removed using an intensity change point algorithm (Ensign and Pande, 2009; O'Donoghue *et al.*, 2013) to identify changes in intensity over the duration of the trajectory. This algorithm uses a Bayesian model-selection technique to identify discrete changes of mean intensity for sequences of Poisson-distributed data. The only parameter for the model is a Bayes factor used in a recursive decision procedure to divide each trajectory into segments of constant mean intensity. Parameters for mNG were determined in Schwartz *et al.* (2017).

### TIRF microscopy optical setup for two-color correlation

TIRF imaging data were collected using an inverted microscope (IX83; Olympus) equipped with a 60×/1.5 NA oil-immersion TIRF (UPlanApo; Olympus). Fluorescence excitation used a 640 nm/140 mW diode laser (Olympus Soft Imaging Solution; 00026121) and a 488 nm/100 mW diode laser (Olympus Soft Imaging Solution; 00026125). Images were captured using a Hamamatsu ORCA-Fusion sCMOS camera (C14440) and Hamamatsu W-View Gemini image splitter (A12801-01) for two-color simultaneous live cell acquisition; a filter set of Semrock single-bandpass 675/67 nm (FF02-675/67) and a Semrock 520/28 nm (FF02-520/28) were used in combination with a Semrock single-edge standard epifluorescence dichroic beamsplitter (FF555-Di03). Images were acquired at 60 s intervals (500 ms exposure time). Samples were maintained at 35°C using a Bioptechs objective heater.

### BAMF image analysis

We used BAMF (Fazel *et al.*, 2019) to process the acquired raw image frames of IgE and Syk to localize the emitters as well as classifying them into signal (in-focus) and background (out-of-focus) emitters. The signal emitters found by BAMF were used to reconstruct background/noise-free images of IgE aggregates. The obtained noise-free images of IgE were then used to define the borders of IgE aggregates using a Sobel filter for edge detection (Bovik, 2009). Given the edges of the IgE aggregates, we determined whether corresponding Syk molecules resided within distinct IgE aggregate

borders. Syk emitters inside the borders of IgE aggregates were identified by eliminating all emitters whose location was either smaller or larger than the coordinates of the defined IgE aggregate border. The intensity associated with each Syk cluster or IgE aggregate was found by summing the intensities of all Syk molecules determined to be located inside the respective IgE aggregate border or by summing the intensities of IgE molecules defined to be in a given aggregate. The intensity of the IgE aggregates was then plotted against the intensity of the corresponding Syk molecules.

### Flow cytometry receptor level comparison

Cells were incubated with 1 μg/ml fluorescently labeled IgE (AF647; Thermo Fisher Scientific) overnight, with a population left unlabeled as the negative control. The level of FcεRI expression for cell populations was determined using an Accuri C6 Plus cytometer (BD Biosciences).

### Immunoblotting

Cells ($4 \times 10^6$) were plated on 100 mm tissue-grade culture plates and primed overnight with 1 μg/ml IgE. Cells were stimulated with respective antigen or mock for the indicated times at 37°C in Hank's buffered saline. Cells were rinsed in cold phosphate-buffered saline and lysed on ice for 20 min with NP-40 lysis buffer (150 nM NaCl, 50 mM Tris, 1% NP-40) in the presence of Halt Protease and Phosphatase inhibitors (Thermo Fisher Scientific). Lysates were cleared by centrifugation at 13,000 × *g* for 10 min at 4°C. Protein concentrations were determined by BCA assay (Thermo Fisher Scientific), and 25 μg was loaded into polyacrylamide gels. Whole lysates or immunoprecipitated samples were boiled with reducing sample buffer, except for lysates used for the detection of FcεRIγ phosphorylation where nonreducing sample buffer was used to preserve the γ-dimer. Proteins were transferred from the SDS–PAGE gel to nitrocellulose membranes using the iBlot2 system (Life Technologies). Membranes were blocked for 30 min in 3% bovine serum albumin (BSA)/0.1% Tween-20/ tris buffered saline (TBS) and probed overnight with primary antibodies at 4°C. HRP-conjugated secondary antibodies were used for detection and incubated with membranes for 1 h at RT. Membranes were imaged on the Odyssey Blot Imager (Li-Cor). Analysis was performed using ImageStudio software.

### Immunoprecipitation

Paired cell lysates were immunoprecipitated by first incubating lysates with the respective antibody at 4°C for 1 h, rotating. Protein A/G PLUS-Agarose (Santa Cruz; sc-2003) was added after the initial antibody incubation, and samples were then incubated again at 4°C overnight, rotating. Samples were then centrifuged at 2500 × *g* for 3 min at 4°C for subsequent washes with NP-40 lysis buffer, again in the presence of Halt Protease and Phosphatase inhibitors (Thermo Fisher Scientific). Samples were boiled in 2× sample buffer (BioRad; 1658063).

### Statistical analysis

Analysis of calcium data and SPT was performed using in-house MATLAB code described previously (Schwartz *et al.*, 2017). The amplitude of calcium response and lag time are presented as mean and SEM. Off-rate error bars indicate standard error, which are calculated as the square root of the variance of the posterior probability distribution generated by the Markov chain. Statistical tests for comparison between groups was completed as indicated in the figure legends and was performed using GraphPad (San Diego, CA) Prism software and graph formatting, and *t* tests were completed using Microsoft Excel. The Kruskal–Wallis test that does not assume a normal distribution was completed using MATLAB.

### Code availability

All computer code is available upon request.

## ACKNOWLEDGMENTS

This work was supported by National Institutes of Health grants R35GM126934, R01GM114075, and P50GM085273. This research was partially supported by University of New Mexico Comprehensive Cancer Center Support Grant NCI P30CA118100 and made use of the Fluorescence Microscopy and Cell Imaging and the Flow Cytometry Shared Resources. We thank John Cambier for sharing the G410 anti-pY antibody. We thank Rachel Grattan for assistance with cell culture and reagent preparation, Samantha L. Schwartz, David J. Schodt, and Michael J. Wester for assistance with experimental methods and data analysis and Derek Rinaldi for assistance with calcium imaging and useful comments on the manuscript. Thank you also to Cheryl A. Telmer for generation of the Syk(SH2)-SYFP2 construct and Luke Lavish for the JF646 dye.

## REFERENCES

Adamczewski M, Numerof RP, Koretzky GA, Kinet JP (1995). Beta-and gamma-chains. Phosphorylation of high affinity IgE receptor regulation by CD45 of the tyrosine. J Immunol 154, 3047–3055.

Andrews NL, Pfeiffer JR, Martinez AM, Haaland DM, Davis RW, Kawakami T, Oliver JM, Wilson BS, Lidke DS (2009). Small, mobile FcεRI receptor aggregates are signaling competent. Immunity 31, 469–479.

Antenucci L, Hytönen VP, Ylänne J (2018). Phosphorylated immunoreceptor tyrosine-based activation motifs and integrin cytoplasmic domains activate spleen tyrosine kinase via distinct mechanisms. J Biol Chem 293, 4591–4602.

Bauer B, Steinle A (2017). HemITAM: a single tyrosine motif that packs a punch. Sci Signal 10, eaan3679.

Bauer B, Wotapek T, Zöller T, Rutkowski E, Steinle A (2017). The activating C-type lectin-like receptor NKp65 signals through a hemi-immunoreceptor tyrosine-based activation motif (hemITAM) and spleen tyrosine kinase (Syk). J Biol Chem 292, 3213–3223.

Bovik AC (2009). The Essential Guide to Image Processing, Amsterdam, Netherlands: Elsevier.

Brazin KN, Mallis RJ, Boeszoermenyi A, Feng Y, Yoshizawa A, Reche PA, Kaur P, Bi K, Hussey RE, Duke-Cohan JS, *et al.* (2018). The T cell antigen receptor α transmembrane domain coordinates triggering through regulation of bilayer immersion and CD3 subunit associations. Immunity 49, 829–841.e6.

Chakraborty AK, Weiss A (2014). Insights into the initiation of TCR signaling. Nat Immunol 15, 798–807.

Chan VWF, Meng F, Soriano P, DeFranco AL, Lowell CA (1997). Characterization of the B lymphocyte populations in lyn-deficient mice and the role of lyn in signal initiation and down-regulation. Immunity 7, 69–81.

Chong ZZ, Maiese K (2007). The Src homology 2 domain tyrosine phosphatases SHP-1 and SHP-2: diversified control of cell growth, inflammation, and injury. Histol Histopathol 22, 1251–1267.

Chu DH, Spits H, Peyron JF, Rowley RB, Bolen JB, Weiss A (1996). The Syk protein tyrosine kinase can function independently of CD45 or Lck in T cell antigen receptor signaling. EMBO J 15, 6251–6261.

Deindl S, Kadlecek TA, Brdicka T, Cao X, Weiss A, Kuriyan J (2007). Structural basis for the inhibition of tyrosine kinase activity of ZAP-70. Cell 129, 735–746.

Ensign DL, Pande VS (2009). Bayesian detection of intensity changes in single molecule and molecular dynamics trajectories. J Phys Chem B 114, 280–292.

Faeder JR, Hlavacek WS, Reischl I, Blinov ML, Metzger H, Redondo A, Wofsy C, Goldstein B (2003). Investigation of early events in FcεRI-mediated signaling using a detailed mathematical model. J Immunol 170, 3769–3781.

Fasbender F, Claus M, Wingert S, Sandusky M, Watzl C (2017). Differential requirements for Src-family kinases in SYK or ZAP70-mediated SLP-76 phosphorylation in lymphocytes. Front Immunol 8, 789.

Fazel M, Wester MJ, Mazloom-Farsibaf H, Meddens MBM, Eklund AS, Schlichthaerle T, Schueder F, Jungmann R, Lidke KA (2019). Bayesian multiple emitter fitting using reversible jump Markov chain Monte Carlo. Sci Rep 9, 1–10.

Feng Y, Reinherz EL, Lang MJ (2018). αβ T cell receptor mechanosensing forces out serial engagement. Trends Immunol 39, 596–609.

Furumoto Y, Nunomura S, Terada T, Rivera J, Ra C (2004). The FcεRIbeta immunoreceptor tyrosine-based activation motif exerts inhibitory control on MAPK and IkappaB kinase phosphorylation and mast cell cytokine production. J Biol Chem 279, 49177–49187.
Fütterer K, Wong J, Grucza RA, Chan AC, Waksman G (1998). Structural basis for Syk tyrosine kinase ubiquity in signal transduction pathways revealed by the crystal structure of its regulatory SH2 domains bound to a dually phosphorylated ITAM peptide. J Mol Biol 281, 523–537.
Gaul BS, Harrison ML, Geahlen RL, Burton RA, Post CB (2000). Substrate recognition by the Lyn protein-tyrosine kinase: NMR structure of the immunoreceptor-tyrosine-based activation motif signaling region of the B cell antigen receptor. J Biol Chem 275, 16174–16182.
Geahlen RL (2009). Syk and pTyr'd: signaling through the B cell antigen receptor. Biochim Biophys Acta 1793, 1115–1127.
Gimborn K, Lessmann E, Kuppig S, Krystal G, Huber M (2005). SHIP down-regulates FcεR1-induced degranulation at supraoptimal IgE or antigen levels. J Immunol 174, 507–516.
Hatada MH, Lu X, Laird ER, Green J, Morgenstern JP, Lou M, Marr CS, Phillips TB, Ram MK, Theriault K, *et al.* (1995). Molecular basis for interaction of the protein tyrosine kinase ZAP-70 with the T-cell receptor. Nature 377, 27–31.
Hernandez-Hansen V, Smith AJ, Surviladze Z, Chigaev A, Mazel T, Kalesnikoff J, Lowell CA, Krystal G, Sklar LA, Wilson BS, *et al.* (2004). Dysregulated FcεRI signaling and altered Fyn and SHIP activities in Lyn-deficient mast cells. J Immunol 173, 100–112.
Hibbs ML, Tarlinton DM, Armes J, Grail D, Hodgson G, Maglitto R, Stacker SA, Dunn AR (1995). Multiple defects in the immune system of Lyn-deficient mice, culminating in autoimmune disease. Cell 83, 301–311.
Ho SN, Hunt HD, Horton RM, Pullen JK, Pease LR (1989). Site-directed mutagenesis by overlap extension using the polymerase chain reaction. Gene 77, 51–59.
Huang J, Brameshuber M, Zeng X, Xie J, Li QJ, Chien YH, Valitutti S, Davis MM (2013). A single peptide-major histocompatibility complex ligand triggers digital cytokine secretion in CD4+ T cells. Immunity 39, 846–857.
Huber M, Helgason CD, Damen JE, Liu L, Humphries RK, Krystal G (1998). The src homology 2-containing inositol phosphatase (SHIP) is the gatekeeper of mast cell degranulation. Proc Natl Acad Sci USA 95, 11330–11335.
Hughes CE, Pollitt AY, Mori J, Eble JA, Tomlinson MG, Hartwig JH, O'Callaghan CA, Fütterer K, Watson SP (2010). CLEC-2 activates Syk through dimerization. Blood 115, 2947–2955.
Huysamen C, Willment JA, Dennehy KM, Brown GD (2008). CLEC9A is a novel activation C-type lectin-like receptor expressed on BDCA3+ dendritic cells and a subset of monocytes. J Biol Chem 283, 16693–16701.
Johnson SA, Pleiman CM, Pao L, Schneringer J, Hippen K, Cambier JC (1995). Phosphorylated immunoreceptor signaling motifs (ITAMs) exhibit unique abilities to bind and activate Lyn and Syk tyrosine kinases. J Immunol 155, 4596–4603.
Kalesnikoff J, Galli SJ (2008). New developments in mast cell biology. Nat Immunol 9, 1215–1223.
Kawakami Y, Kitaura J, Satterthwaite AB, Kato RM, Asai K, Hartman SE, Maeda-Yamamoto M, Lowell CA, Rawlings DJ, Witte ON, Kawakami T (2000). Redundant and opposing functions of two tyrosine kinases, Btk and Lyn, in mast cell activation. J Immunol 165, 1210–1219.
Kihara H, Siraganian RP (1994). Src homology 2 domains of Syk and Lyn bind to tyrosine-phosphorylated subunits of the high affinity IgE receptor. J Biol Chem 269, 22427–22432.
Kim YM, Pan JYJ, Korbel GA, Peperzak V, Boes M, Ploegh HL (2006). Monovalent ligation of the B cell receptor induces receptor activation but fails to promote antigen presentation. Proc Natl Acad Sci USA 103, 3327–3332.
Kimura T, Kihara H, Bhattacharyya S, Sakamoto H, Appella E, Siraganian RP (1996a). Downstream signaling molecules bind to different phosphorylated immunoreceptor tyrosine-based activation motif (ITAM) peptides of the high affinity IgE receptor. J Biol Chem 271, 27962–27968.
Kimura T, Sakamoto H, Appella E, Siraganian RP (1996b). Conformational changes induced in the protein tyrosine kinase p72syk by tyrosine phosphorylation or by binding of phosphorylated immunoreceptor tyrosine-based activation motif peptides. Mol Cell Biol 16, 1471–1478.
Kimura T, Sakamoto H, Appella E, Siraganian RP (1997). The negative signaling molecule SH2 domain-containing inositol-polyphosphate 5-phosphatase (SHIP) binds to the tyrosine-phosphorylated β subunit of the high affinity IgE receptor. J Biol Chem 272, 13991–13996.
Kovářová M, Tolar P, Arudchandran R, Dráberová L, Rivera J, Dráber P (2001). Structure-function analysis of Lyn kinase association with lipid rafts and initiation of early signaling events after Fc receptor I aggregation. Mol Cell Biol 21, 8318–8328.
Krogsgaard M, Juang J, Davis MM (2007). A role for "self" in T-cell activation. Semin Immunol 19, 236–244.
Letourneur F, Klausner RD (1991). T-cell and basophil activation through the cytoplasmic tail of T-cell-receptor ζ family proteins. Proc Natl Acad Sci USA 88, 8905–8909.
Li HL, Davis WW, Whiteman EL, Birnbaum MJ, Puré E (1999). The tyrosine kinases Syk and Lyn exert opposing effects on the activation of protein kinase Akt/PKB in B lymphocytes. Proc Natl Acad Sci USA 96, 6890–6895.
Liu FT, Bohn JW, Ferry EL, Yamamoto H, Molinaro CA, Sherman LA, Klinman NR, Katz DH (1980). Monoclonal dinitrophenyl-specific murine IgE antibody: preparation, isolation, and characterization. J Immunol 124, 2728–2737.
Ma H, Yankee TM, Hu J, Asai DJ, Harrison ML, Geahlen RL (2001). Visualization of Syk-antigen receptor interactions using green fluorescent protein: differential roles for Syk and Lyn in the regulation of receptor capping and internalization. J Immunol 166, 1507–1516
Ma Y, Poole K, Goyette J, Gaus K (2017). Introducing membrane charge and membrane potential to T cell signaling. Front Immunol 8, 1.
Mahajan A, Barua D, Cutler P, Lidke DS, Espinoza FA, Pehlke C, Grattan R, Kawakami Y, Tung C-SS, Bradbury ARMM, *et al.* (2014). Optimal aggregation of FcεRI with a structurally defined trivalent ligand overrides negative regulation driven by phosphatases. ACS Chem Biol 9, 1508–1519.
Mainou B, Dermody T (2011). Src kinase mediates productive endocytic sorting of reovirus during cell entry. J Virol 85, 3203–3213.
Mendoza GR, Minagawa K (1982). Subthreshold and suboptimal desensitization of human basophils. II. Nonspecificity and irreversibility of desensitization. Int Arch Allergy Appl Immunol 69, 282–284.
Metzger H, Alcaraz G, Hohman R, Kinet JP, Pribluda V, Quarto R (1986). The receptor with high affinity for immunoglobulin E. Annu Rev Immunol 4, 419–470.
Mukherjee S, Zhu J, Zikherman J, Parameswaran R, Kadlecek TA, Wang Q, Au-Yeung B, Ploegh H, Kuriyan J, Das J, Weiss A (2013). Monovalent and multivalent ligation of the B cell receptor exhibit differential dependence upon Syk and Src family kinases. Sci Signal 6, ra1.
Narula SS, Yuan RW, Adams SE, Green OM, Green J, Philips TB, Zydowsky LD, Botfield MC, Hatada M, Laird ER, *et al.* (1995). Solution structure of the C-terminal SH2 domain of the human tyrosine kinase Syk complexed with a phosphotyrosine pentapeptide. Structure 3, 1061–1073.
Nishizumi H, Taniuchi I, Yamanashi Y, Kitamura D, Ilic D, Mori S, Watanabe T, Yamamoto T (1995). Impaired proliferation of peripheral B cells and indication of autoimmune disease in lyn-deficient mice. Immunity 3, 549–560.
Nishizumi H, Yamamoto T (1997). Impaired tyrosine phosphorylation and Ca2+ mobilization, but not degranulation, in lyn-deficient bone marrow-derived mast cells. J Immunol 158, 2350–2355.
Nunes de Miranda SM, Wilhelm T, Huber M, Zorn CN (2016). Differential Lyn-dependence of the SHIP1-deficient mast cell phenotype. Cell Commun Signal 14, 12.
O'Donoghue GP, Pielak RM, Smoligovets AA, Lin JJ, Groves JT (2013). Direct single molecule measurement of TCR triggering by agonist pMHC in living primary T cells. eLife 2, e00778.
O'Neill SK, Getahun A, Gauld SB, Merrell KT, Tamir I, Smith MJ, Dal Porto JM, Li Q-Z, Cambier JC (2011). Monophosphorylation of CD79a and CD79b ITAM motifs initiates a SHIP-1 phosphatase-mediated inhibitory signaling cascade required for B cell anergy. Immunity 35, 746–756.
Ono M, Bolland S, Tempst P, Ravetch JV (1996). Role of the inositol phosphatase SHIP in negative regulation of the immune system by the receptor FcγRIIB. Nature 383, 263–266.
Pao LI, Cambier JC (1997). Syk, but not Lyn, recruitment to B cell antigen receptor and activation following stimulation of CD45- B cells. J Immunol 158, 2663–2669.
Park MJ, Sheng R, Silkov A, Jung DJ, Wang ZG, Xin Y, Kim H, Thiagarajan-Rosenkranz P, Song S, Yoon Y, *et al.* (2016). SH2 domains serve as lipid-binding modules for pTyr-signaling proteins. Mol Cell 62, 7–20.
Parravicini V, Gadina M, Kovarova M, Odom S, Gonzalez-Espinosa C, Furumoto Y, Saitoh S, Samelson LE, O'shea JJ, Rivera J (2002). Fyn kinase initiates complementary signals required for IgE-dependent mast cell degranulation. Nat Immunol 3, 741–748.
Ra C, Nunomura S, Okayama Y (2012). Fine-tuning of mast cell activation by FceRIß chain. Front Immunol 3, 112.
Rogers NC, Slack EC, Edwards AD, Nolte MA, Schulz O, Schweighoffer E, Williams DL, Gordon S, Tybulewicz VL, Brown GD, *et al.* (2005).

Syk-dependent cytokine induction by dectin-1 reveals a novel pattern recognition pathway for C type lectins. Immunity 22, 507–517.
Rolli V, Gallwitz M, Wossning T, Flemming A, Schamel WWAA, Zürn C, Reth M (2002). Amplification of B cell antigen receptor signaling by a Syk/ITAM positive feedback loop. Mol Cell 10, 1057–1069.
Sanderson MP, Wex E, Kono T, Uto K, Schnapp A (2010). Syk and Lyn mediate distinct Syk phosphorylation events in FcεRI-signal transduction: implications for regulation of IgE-mediated degranulation. Mol Immunol 48, 171–178.
Schwartz SL, Cleyrat C, Olah MJ, Relich PK, Phillips GK, Hlavacek WS, Lidke KA, Wilson BS, Lidke DS (2017). Differential mast cell outcomes are sensitive to FcεRI-Syk binding kinetics. Mol Biol Cell 28, 3397–3414.
Shelby SA, Holowka D, Baird B, Veatch SL (2013). Distinct stages of stimulated FcεRI receptor clustering and immobilization are identified through superresolution imaging. Biophys J 105, 2343–2354.
Shi X, Bi Y, Yang W, Guo X, Jiang Y, Wan C, Li L, Bai Y, Guo J, Wang Y, *et al*. (2012). Ca2+ regulates T-cell receptor activation by modulating the charge property of lipids. Nature 493, 111–115.
Shiue L, Zoller MJ, Brugge JS (1995). Syk is activated by phosphotyrosine-containing peptides representing the tyrosine-based activation motifs of the high affinity receptor for IgE. J Biol Chem 270, 10498–10502.
Sigalov AB (2004). Multichain immune recognition receptor signaling: different players, same game? Trends Immunol 25, 583–589.
Siraganian RP, de Castro RO, Barbu EA, Zhang J (2010). Mast cell signaling: the role of protein tyrosine kinase Syk, its activation and screening methods for new pathway participants. FEBS Lett 584, 4933–4940.
Siraganian RP, Zhang J, Suzuki K, Sada K (2002). Protein tyrosine kinase Syk in mast cell signaling. Mol Immunol 38, 1229–1233.
Starlets D, Gore Y, Binsky I, Haran M, Harpaz N, Shvidel L, Becker-Herman S, Berrebi A, Shachar I (2006). Cell-surface CD74 initiates a signaling cascade leading to cell proliferation and survival. Blood 107, 4807–4816.
Suzuki R (2017). The emerging picture of mast cell activation: the complex regulatory network of high-affinity receptor for immunoglobulin E signaling. Biol Pharm Bull 40, 1828–1832.
Suzuki T, Kono H, Hirose N, Okada M, Yamamoto T, Yamamoto K, Honda Z (2000). Differential involvement of Src family kinases in Fcγ receptor-mediated phagocytosis. J Immunol 165, 473–482.
Takata M, Sabe H, Hata A, Inazu T, Homma Y, Nukada T, Yamamura H, Kurosaki T (1994). Tyrosine kinases Lyn and Syk regulate B cell receptor-coupled Ca2+ mobilization through distinct pathways. EMBO J 13, 1341–1349.
Travers T, Kanagy WK, Mansbach RA, Jhamba E, Cleyrat C, Goldstein B, Lidke DS, Wilson BS, Gnanakaran S (2019). Combinatorial diversity of Syk recruitment driven by its multivalent engagement with FcεRIγ. Mol Biol Cell 30, 2331–2347.
Turner H, Kinet J-P (1999). Signalling through the high-affinity IgE receptor FceRI. Nature 402, 24–30.
Watson AA, Christou CM, James JR, Fenton-May AE, Moncayo GE, Mistry AR, Davis SJ, Gilbert RJC, Chakera A, O'Callaghan CA (2009). The platelet receptor CLEC-2 is active as a dimer. Biochemistry 48, 10988–10996.
Wilson BS, Kapp N, Lee RJ, Pfeiffer JR, Martinez AM, Platt Y, Letourneur F, Oliver JM (1995). Distinct functions of the Fc epsilon R1 gamma and beta subunits in the control of FcεR1-mediated tyrosine kinase activation and signaling responses in RBL-2H3 mast cells. J Biol Chem 270, 4013–4022.
Wilson BS, Pfeiffer JR, Oliver JM (2000). Observing FcεRI signaling from the inside of the mast cell membrane. J Cell Biol 149, 1131–1142.
Xiao W, Nishimoto H, Hong H, Kitaura J, Nunomura S, Maeda-Yamamoto M, Kawakami Y, Lowell CA, Ra C, Kawakami T (2005). Positive and negative regulation of mast cell activation by Lyn via the FcεRI. J Immunol 175, 6885–6892.
Yamashita T, Suzuki R, Backlund PS, Yamashita Y, Yergey AL, Rivera J (2008). Differential dephosphorylation of the FcRgamma immunoreceptor tyrosine-based activation motif tyrosines with dissimilar potential for activating Syk. J Biol Chem 283, 28584–28594.
Yanagi S, Sugawara H, Kurosaki M, Sabe H, Yamamura H, Kurosaki T (1996). CD45 modulates phosphorylation of both autophosphorylation and negative regulatory tyrosines of Lyn in B cells . J Biol Chem 271, 30487–30492.
Yokosuka T, Sakata-Sogawa K, Kobayashi W, Hiroshima M, Hashimoto-Tane A, Tokunaga M, Dustin ML, Saito T (2005). Newly generated T cell receptor microclusters initiate and sustain T cell activation by recruitment of Zap70 and SLP-76. Nat Immunol 6, 1253–1262.
Young RM, Holowka D, Baird B (2003). A lipid raft environment enhances Lyn kinase activity by protecting the active site tyrosine from dephosphorylation. J Biol Chem 278, 20746–20752.
Zhang J, Berenstein EH, Evans RL, Siraganian RP (1996). Transfection of Syk protein tyrosine kinase reconstitutes high affinity IgE receptor-mediated degranulation in a Syk-negative variant of rat basophilic leukemia RBL-2H3 cells. J Exp Med 184, 71–79.